Human CCR4-NOT is a global regulator of gene expression and is a novel silencer of retrotransposon activation

Shardul Kulkarni[1,2], Alexis Morrissey[1,2], Aswathy Sebastian[4], Cheryl A. Keller[2,5], Belinda Giardine[2], Courtney Smith[1,2], Oluwasegun T. Akinniyi[1,2], Alexei Arnaoutov[3], Istvan Albert[2,4], Shaun Mahony[1,2], Joseph C. Reese*[1,2]

Affiliations

[1]Center for Eukaryotic Gene Regulation and [2]Department of Biochemistry and Molecular Biology, The Pennsylvania State University, University Park, PA, 16802 USA.

[3]Division of Molecular and Cellular Biology, National Institute of Child Health and Human Development, National Institutes of Health, Bethesda, MD, 20892 USA.

[4]Huck Institutes of the Life Sciences, Pennsylvania State University, University Park, Pennsylvania, 16802 USA.

[5]Genomics Research Incubator, Pennsylvania State University, University Park, Pennsylvania, 16802 USA

* **Corresponding Author:**
Joseph C. Reese
Center for Eukaryotic Gene Regulation
Biochemistry and Molecular Biology
Penn State University
463A North Frear Laboratory
University Park, PA, 16802
Jcr8@psu.edu
(814) 865-1976

Running title: CCR4-NOT regulates global gene expression through KZFPs

Keywords: CCR4-NOT, Krab Zinc finger proteins (KZFPs), Retrotransposons, LINE elements, transcription

Abstract

CCR4-NOT regulates multiple steps in gene regulation, including transcription, mRNA decay, protein ubiquitylation, and translation. It has been well studied in budding yeast; however, relatively less is known about its regulation and functions in mammals. To characterize the functions of the human CCR4-NOT complex, we developed a rapid auxin-induced degron system to deplete CNOT1 (the scaffold of the complex) and CNOT4 (E3 ubiquitin ligase) in cell culture. Transcriptome-wide measurements of gene-expression revealed that depleting CNOT1 changed several thousand transcripts, wherein most mRNAs were increased and resulted in a global decrease in mRNA decay rates. In contrast to what was observed in CNOT1-depleted cells, CNOT4 depletion only modestly changed RNA steady-state levels and, surprisingly, led to a global acceleration in mRNA decay. To further investigate the role of CCR4-NOT in transcription, we used transient transcriptome sequencing (TT-seq) to measure ongoing RNA synthesis. Depletion of either subunit resulted in increased RNA synthesis of several thousand genes. In contrast to most of the genome, a rapid reduction in the synthesis of KRAB-Zinc-Finger-proteins (KZNFs) genes, especially those clustered on chromosome 19, was observed. KZNFs are transcriptional repressors of retro-transposable elements (rTEs), and consistent with the decreased KZNFs expression, we observed a significant and rapid activation of rTEs, mainly Long interspersed Nuclear Elements (LINEs). Our data reveal that CCR4-NOT regulates gene expression and silences retrotransposons across the genome by maintaining KZNF expression. These data establish CCR4-NOT as a global regulator of gene expression, and we have identified a novel mammalian-specific function of the complex, the suppression of rTEs.

Introduction

CCR4-NOT is a highly conserved complex that regulates multiple steps in of gene expression in the nucleus and cytoplasm. Subunits of the Ccr4-Not complex were first identified and characterized in yeast as regulators of the TATA-binding protein and transcription initiation, but it has since been shown to regulate the elongation stage of transcription and chromatin by regulating the activity of histone modifying complexes (Chalabi Hagkarim and Grand 2020; Miller and Reese 2012; Collart 2016; Collart and Timmers 2004). However, comparatively less is known about its function in metazoans, especially its nuclear functions. In cytoplasm, CCR4-NOT functions as the major mRNA deadenylase that initiates mRNA decay by degrading the 3' poly-A tail. It also associates with ribosomes, where it monitors the translatability of mRNAs and directs the decay of messages that are enriched in non-optimal codons and are those that are untranslatable (Miller and Reese 2012; Shirai et al. 2014; Inada and Makino 2014; Chalabi Hagkarim and Grand 2020; Collart 2016).

Shortening of poly-A tail is, in majority of cases, the rate limiting step in mRNA decay (Eisen et al. 2020; Pavanello et al. 2023; Doidge et al. 2012; Chen and Shyu 2011). In the canonical model, deadenylation at the 3' end of the message by Pan2/Pan3 deadenylase complex is followed by further shortening of poly-A tail by CCR4-NOT complex. The degradation of mRNAs then occurs in either 5'-> 3' direction by Xrn1 after decapping by the Dcp1–Dcp2 complex or in the 3' -> 5' direction by the exosome. Human CCR4-NOT contains one of either CNOT7/CNOT8 DEDD type deadenylases (yCaf1) and one of either CNOT6/CNOT6L exonuclease-endonuclease-phosphatase [EEP] family of deadenylases (yCcr4) (Lau et al. 2009). It is recruited to target mRNAs via RNA binding proteins (RBP) or the miRNA machinery to specific sequences located within the 3'UTRs. The large scaffold subunit CNOT1 is critical to bridge the RBP and the deadenylase subunits to target mRNAs for degradation; thus, plays a critical role in the function and integrity of the complex (Basquin et al. 2012; Petit et al. 2012; Zhang et al. 2022; Keskeny et al. 2019; Chen et al. 2014).

The yeast and mammalian Ccr4-Not complexes have similar overall composition and structures, especially the 'core' subunits, but there are some key differences, including being composed of different subunits (Miller and Reese 2012; Collart 2016; Chalabi Hagkarim and Grand 2020). Another function of the complex is protein ubiquitylation, which is carried out by yNot4/hCNOT4, a RING domain-containing E3 ligase. Yeast Not4p is an integral subunit of the complex (Albert et al. 2002; Panasenko and Collart 2011), but CNOT4 in metazoans does not co-purify with the complex (Lau et al. 2009; Temme et al. 2010). However, it has been shown that recombinant CNOT4 binds to CNOT9, an integral subunit of the complex (Keskeny et al. 2019). Recent biochemical studies revealed that CNOT4 ubiquitylates ribosomes, but given that it is not tightly associated with human CCR4-NOT, its precise functions remain to be determined (Absmeier et al. 2023). A number of studies have interrogated the

function of human CCR4-NOT subunits in the regulation of mRNA degradation using long term (days long) shRNA/RNAi treatments and knockout cell lines and organisms. These studies have mostly focused on its function in mRNA decay by targeting the catalytic deadenylases CNOT6/6L and CNOT7/8 (Vieux and Clarke 2018; Dai et al. 2021; Aslam et al. 2009). Furthermore, a thorough analysis of the roles of CNOT4 in transcription and mRNA decay has not been undertaken. This may be due to the uncertainty, based on multiple co-purification studies, whether CNOT4 is a subunit of the complex.

LINEs (Long Interspersed Nuclear Elements) are abundant retrotransposons that impact a wide range of functions in development, genome integrity and genome evolution (Elbarbary et al. 2016; Kohlrausch et al. 2022). Nearly 20% of the human and mouse genomes are occupied by annotated LINE1 (L1) sequences (Lander et al. 2001) and since L1s are responsible for amplification of other repeat elements like SINEs, L1 activity possibly accounts for as much as 50% of mammalian DNA (Graham and Boissinot 2006). Inappropriate activation of LINE elements has been associated with the instability of genomes, developmental defects, cancer, neurological problems and aging (Beck et al. 2011). Critical for the repression of LINEs are the Kruppel-associated box zinc-finger proteins (KZFPs), the largest family of transcriptional repressors (Ecco et al. 2017). KZFPs bind to their target DNA sequence through their Zinc finger domain and recruits a transcriptional repressor complex, KAP1/TRIM28, through the KRAB domain to silence gene and LINE expression (Bruno et al. 2019). KAP1/TRIM28 corepressor recruits chromatin co-repressors like SETDB1 (histone H3K9me3 methyltransferase) (Schultz et al. 2002), HP1 (Heterochromatin protein 1) (Nielsen et al. 1999; Ryan et al. 1999); and the NuRD complex (deacetylase) (Schultz et al. 2001) to establish heterochromatin over repeat elements. KZFPs also bind near promoters of protein coding genes and endogenous retrovirus LTRs to repress gene expression (Lykoskoufis et al. 2024; Liu et al. 2018; Brattås et al. 2017; Osipovich et al. 2023; Ecco et al. 2016; Guio et al. 2018; Gebrie 2023). These ancient LTRs are conserved and evidence indicate that the KZFP-bound LTRs have been co-opted to regulate genes throughout mammalian genomes (Kunarso et al. 2010; Macfarlan et al. 2012; Chuong et al. 2016). Given the importance of KZFPs in shaping the transcriptional landscape of genomes and the dire consequences of the activation of LINE elements, understanding the mechanisms of LINE silencing is of great importance. Since KZFPs are central to this process, understanding the pathways that regulate their activity is crucial to understand gene expression, development and genome integrity.

We employed an auxin inducible degron (AID) strategy to efficiently and rapidly deplete CNOT1 and CNOT4 to address the function of these critical subunits of the CCR4-NOT complex in gene expression. Our findings confirmed that although CNOT4 does not co-purify with the complex, proximity labeling (BioID) indicates it associates with the complex *in vivo*. We found that depleting CNOT1 stabilized mRNAs in the cell, but remarkably,

depleting CNOT4 had the opposite effect, accelerating mRNA turnover. Thus, CNOT1p and CNOT4p have unique functions. Despite the opposite effects on mRNA stability, depletion of either subunit results in rapid and wide-spread increased transcription, providing the first evidence that human CCR4-NOT regulates transcription. Interestingly, we found that inactivating CCR4-NOT led to the activation LINE and other retrotransposon elements throughout the genome, which correlated with a downregulation of KZFP gene expression. Thus, we have discovered a novel function for CCR4-NOT in regulating genome-wide transcription and maintaining genome integrity by suppressing the activation of repeat transposable elements.

Results

An Auxin inducible degron (AID) system for rapid degradation of human CNOT1 and CNOT4

To study human CCR4-NOT complex, we employed CRISPR/Cas9 gene editing system to biallelically introduce AID at the C-terminus of CNOT1 and CNOT4 in colorectal adenocarcinoma DLD-1^{TIR1+} cells (Supplemental Figure S1A). We focused on the central scaffold subunit CNOT1 and the E3-ubiquitin ligase subunit CNOT4. Genotyping confirmed homozygous insertion of the AID sequence (Supplemental Figure S1B-C). Cells containing AID-tagged subunits displayed normal viability and growth (Supplemental Figure S1D) and adding the AID tag did not affect the expression levels of other subunit proteins (Supplemental Figure S1E-F) in the absence of auxin. Some proteins display constitutive degradation in the absence of auxin, but the expression levels of tagged proteins were comparable to that of untagged proteins (Figure 1A, 1B). Importantly, adding auxin led to a rapid depletion of the tagged proteins and their levels were undetectable within an hour of auxin addition (Figure 1C-D, Supplemental Figure S1G-H).

siRNA mediated partial knockdown of CNOT1 reduced cell growth, induced cell cycle arrest and ultimately apoptotic cell death (Ito et al. 2011; Hagkarim et al. 2023). We examined the effects of rapid depletion of CNOT1 and CNOT4 on cell growth and the cell cycle. Cells with AID tagged subunits had no detectable differences in cell growth in the absence of auxin. Depletion of CNOT1 indeed resulted in no cell growth by 24 h and an increase in death beyond 24 h (Supplemental Figure S2A). In contrast, depletion of CNOT4 had no detectable effect on cell growth until 72 h, but this was observed in the parental cell line indicating that prolonged auxin exposure reduces cell growth (Supplemental Figure S2A). Examination of the cell cycle status by flow cytometry revealed that depletion of CNOT1 for 24 h resulted in an increase of cells in G1/S and a corresponding decrease in cells in the S and G2 phases. Once again, different phenotypes were observed when CNOT4 was depleted: no cell cycle arrest was observed (Supplemental Figure S2B). Given these data, going forward, analysis of depleted cells was conducted within 24 h.

Analysis of the effects of subunit depletion on the integrity of CCR4-NOT

Deleting the genes of subunits of the yeast Ccr4-Not complex and depleting subunits of the human complex by long siRNA treatments caused reduced accumulation of other subunits (Ito et al. 2011; Hagkarim et al. 2023; Maillet et al. 2000), especially when the CNOT1/Not1 scaffold subunit was depleted. To check the effects of rapid CNOT1 and CNOT4 depletion on the levels of other subunits, we treated cells with auxin for 2, 4, 8 and 24 h and analyzed protein levels by immunoblotting. Depleting CNOT1 resulted in decreased levels of CNOT6, CNOT7 and CNOT9, while the levels of CNOT2 and CNOT3 did not change. Depleting CNOT1 caused very rapid destruction of CNOT9, which binds directly to CNOT1 (Keskeny et al. 2019; Chen et al. 2014). Subunits of the nuclease module, CNOT6 and CNOT7, required more than 4 h to reduce their protein levels. Interestingly, the levels of CNOT4 protein were elevated between 8-24 h of CNOT1 depletion (Supplemental Figure S3A). The increase in CNOT4 protein levels in CNOT1-depleted cells may be explained by the stabilization and increased accumulation of CNOT4 mRNA (data not shown). In contrast, depletion of CNOT4 did not affect levels of any of the subunits examined (Supplemental Figure S3B).

Yeast Not4 is stably associated with the Ccr4-Not complex, while mammalian CNOT4 does not co-purify with the complex (Collart 2013; Lau et al. 2009; Albert et al. 2000). However, recombinant CNOT4 associates directly with CNOT9 (Keskeny et al. 2019), suggesting CNOT4 may interact with CCR4-NOT, but immunopurification (IP) conditions did not preserve this interaction. We re-evaluated the association of CNOT4 with the complex using size exclusion chromatography (SEC) on lysates, which is considered less disruptive than IP conditions. Furthermore, we used SEC to determine the effects of subunit depletion on CCR4-NOT complex integrity by monitoring the elution of subunits from the column (Figures 2A, B). We chose a depletion time of 4 h because all subunits of the complex, except CNOT9, were still detected in extracts of CNOT1 depleted cells (Supplemental Figure S3 and not shown). In undepleted cells, the CCR4-NOT complex proteins eluted in fractions corresponding to 1 - 1.5 MD molecular weight, MW, (Figures 2A and B; highlighted in red on top), which is comparable to previously reported approximate molecular weight of the complex (Lau et al. 2009). The data also suggested that mere tagging of CNOT1 or CNOT4 with an AID tag does not have adverse effects on the assembly of the complex, which agrees with no changes in protein levels of complex subunits (Supplemental Figure S1E-F). Furthermore, the vast majority of CNOT4 appears to migrate at its calculated MW, ~66Kda, and not with the complex. There is a very weak signal for CNOT4 in the fractions where the complex elutes, but closer examination reveals that depleting CNOT1 did not shift this fraction to lower MW fractions (Figure 2A), suggesting that this small fraction of CNOT4 is not associated with the complex under the conditions used here.

Depletion of the scaffolding protein CNOT1 resulted in the disassembly of the complex ('+auxin' panels in Figure 2A), as evidenced by the elution of CNOT2, CNOT6 and CNOT9 in lower molecular weight fractions. Interestingly, CNOT2 eluted at a significantly higher MW than its calculated MW, 450 kDa versus 60 kDa respectively, suggesting that a subcomplex was formed. Other blots have shown that CNOT3 co-elutes with CNOT2 in these fractions (not shown). Furthermore, in contrast to what was observed when CNOT1 was depleted, depleting CNOT4 had no effect on the integrity of the complex, which eluted at 1-1.5MDa. These data altogether suggest that depletion of CNOT1 leads to disassembly of the complex followed by decreased protein levels of many of its subunits, while depletion of CNOT4 had no obvious effects on the integrity of the CCR4-NOT complex.

Proximity labeling (BioID) indicates CNOT4 associates with CCR4-NOT complex and mRNA regulators *in vivo*

Traditional biochemical methods have not detected CNOT4 in the complex. Even though SEC is not as stringent as immunopurification conditions, it is possible that preparing extracts disrupts the interaction. We applied BioID to investigate the interactome of CNOT1 and CNOT4 in cells and detects transient or weak interactions undetectable by other purification methods (Sears et al. 2019). The sequence coding for biotin ligase (TurboID, TID or miniTurboID, mTID) was inserted at the genomic locus of CNOT1 and CNOT4 (Supplemental Figure S4A). TID is the more active of the two enzymes (Branon et al. 2018). We isolated multiple clones expressing CNOT4^{TID}; however, we could not isolate a clone expressing CNOT1^{TID}, so we used the mTID version (Supplemental Figure S4B). The expression levels of tagged proteins were comparable to that of untagged proteins and treatment with 100 µM biotin did not alter the expression levels of the tagged protein (Supplemental Figure S4C-D). To identify proteins associated with CNOT1^{mTID} and CNOT4^{TID}, we treated cells with 100 µM biotin for 60 min followed by cell lysis and enrichment of biotinylated proteins on streptavidin beads, followed by trypsin digestion. The peptides were labeled with TMT isobaric peptide labeling reagents. Analysis by quantitative mass spectrometry was performed to quantify the proteins labeled by CNOT1^{mTID} or CNOT4^{TID} versus those from parental cells. Each experimental condition had 2 biological replicates, which displayed high correlation in peptide abundances ($R = 0.99$, Supplemental Figure S4E). Proteins showing enrichment of ≥ 1.5-fold and $P^{adj} < 0.05$ were identified as putative interacting proteins. 31 CNOT1 interacting proteins were identified, with 9 of the 12 CCR4-NOT complex proteins showing significant enrichment (Figure 3A, Supplemental Table S1). Three other subunits (CNOT4, CNOT8 and CNOT11) were also shown to be enriched, but did not meet the cutoff criteria. Labeling of CNOT4 by CNOT1^{mTID} suggested that CNOT4 indeed associates with the complex *in vivo*. This was further strengthened by the finding that 11 of 12 subunits of the CCR4-NOT complex were enriched in the CNOT4^{TID} data set (Figure 3B, Supplemental Table S1). We then performed gene ontology (GO) analysis on the CNOT1^{mTID} and CNOT4^{TID} interacting proteins and found that they were enriched with proteins involved in post-transcriptional regulation of RNA expression and

are components of cytoplasmic stress granules, P-body and miRNA complexes (Figure 3C, D). Additionally, the proteins labeled by CNOT1^{mTID} and CNOT4^{TID} showed a highly significant overlap, further strengthening the conclusion that CNOT4 indeed associates with CCR4-NOT complex (Figure 3E). Not surprisingly, BioID of yeast Not1 and Not4, also revealed the complex predominantly associated with cytoplasmic mRNA binding post-transcriptional regulatory proteins (Pfannenstein et al. 2024). A recent study was conducted with 119 human proteins involved in multiple steps of mRNA metabolism (Youn et al. 2018). The authors used the "first generation" biotin ligase (BirA*) fused to the bait proteins. Several of these BirA-Bait proteins, including subunits of CCR4-NOT complex, showed a significant interaction (FDR < 0.05) with CNOT4 (data not shown). Thus, although CNOT4 does not co-purify with the complex, it associates with it in cells and functions in similar pathways.

Depletion of CNOT1 and CNOT4 has distinct effects on steady-state RNA levels.

We examined the effects of depleting CNOT1 or CNOT4 on gene expression by measuring steady-state RNA levels. Parental cells (DLD-1^{TIR1+}), CNOT1^{AID} and CNOT4^{AID} cells were treated with auxin for 2-, 8- and 24-h. Since CCR4-NOT plays a broad role in mRNA stability, ERCC-spike-in control RNAs was used to normalize the data. The biological replicates of each condition showed high correlation (R > 0.99, Supplemental Table S2). We first confirmed that introducing the AID tag (-auxin) did not affect gene expression, which it did not. RNA expression profiles in untagged versus AID tagged cells in the absence of auxin correlated very highly (R > 0.98, Supplemental Table S2). We also checked auxin dependent changes in gene expression in parental cells (untagged strain) and found very few genes with differential expression (N < 10) when exposed to auxin (Supplemental Figure S5A-B).

Differential expression analysis between ±auxin treated AID-tagged cells at each time point was conducted and the number of genes meeting an arbitrary cutoff (FC ≥ 1.5, P^{adj} < 0.01) was calculated. Depleting CNOT1 led to predominantly increased expression over time (Figure 4A-C, top panels for CNOT1^{AID}, Supplemental Figure S5C), consistent with CNOT1's role in mRNA deadenylation [see below and (Ito et al. 2011; Pavanello et al. 2018)]. Greater than 90% of the differentially expressed genes (DEGs) were protein coding genes (Supplemental Figure S5D). In contrast to what was observed in CNOT1-depleted cells, depletion of CNOT4 showed relatively mild effects on steady-state levels of RNAs (Figure 4A-C, bottom panels for CNOT4^{AID}), although more RNAs increased than decreased similar what was observed when CNOT1 was depleted (Supplemental Figure S5C). The differences in gene expression changes in CNOT1- versus CNOT4-depleted cells may be explained in part by the effects of each depletion on complex integrity (Figure 2). Depleting CNOT4 left the complex intact, maintaining CCR4-NOT's deadenylation activity, while depleting CNOT1 destroyed the complex and led to the degradation of multiple subunits. We performed gene ontology (GO) analysis on the genes showing differential changes in expression. The top categories returned for DEGs at all time points in CNOT1 depleted cells were related to transcriptional

regulation of genes (Supplemental Figure S6A). Depletion of CNOT4 for 2 h indeed resulted in DEGs that were involved in transcriptional regulation as well, but later timepoints resulted in no significant enrichment (24 h depletion) of these terms, and genes that were involved in cell cycle regulation showed significant enrichment (Supplemental Figure S6B). This was unexpected since CNOT4 depleted cells showed no cell cycle arrest (Supplemental Figure S2B). Further, genes involved in cell cycle regulation were indeed enriched in CNOT1 depletion (24 h) DEGs' dataset (enrichment FDR = 5.7E-31) which was consistent with arrest of CNOT1-depleted at G1/S transition (Supplemental Figure S2B). Although, there was a stark difference in mRNA expression phenotypes of CNOT1- and CNOT4-depleted cells (Figure 4), there was a strong and significant overlap in DEGs under 2 and 24 h depletion of CNOT1 and CNOT4 (Supplemental Figure S6C-D). These data suggested that these proteins indeed regulate steady state expression of some of the same genes.

CNOT1-depletion causes increased-, while CNOT4 depletion results in decreased – RNA stability.

Steady state mRNA levels are affected by changes in both mRNA decay and synthesis rates. To gain more insights into CCR4-NOT's role in regulating RNA stability, we performed transcriptome-wide measurements of RNA half-lives. Triptolide (TPL), which has been shown to inhibit overall transcription by targeting TFIIH (Titov et al. 2011; Wang et al. 2011) and has been used to calculate RNA half-lives transcriptome-wide, (Gillen et al. 2021). RNA synthesis was inhibited in depleted cells, the levels of RNAs were measured at different timepoints (3, 6 and 12 h) and RNA half-lives were calculated from the data (Figure 5A). The biological replicates of the RNA- seq data showed high correlation (R > 0.93, Supplemental Table S2). The estimated half-lives obtained in this study in parental (un-depleted) cells correlated well with previously published datasets (Arango et al. 2018; Tani et al. 2012; Gillen et al. 2021; Narula et al. 2019; Poetz et al. 2021) (Supplemental Figure S7A). Consistent with CCR4-NOT's role in deadenylation and mRNA decay, depleting CNOT1 resulted in a global stabilization of RNAs (Figure 5B). Boxplot analysis showed that the median half-life of mRNAs under control conditions was 10.6 h, and depleting CNOT1 extended the median half-life to 24.3 h (Figure 5D). Surprisingly, depleting CNOT4 actually increased the rate of RNA turnover (Figure 5C), reducing the median half-life to 6.5 h (Figure 5D). Cumulative fraction analysis further confirmed these findings (Figure 5E). Although CNOT1 and CNOT4 are subunits of the same complex, their respective depletion conferred opposite effects on mRNA stability. The results suggest that CNOT4 is a global attenuator of RNA decay (see discussion). The effects of depleting CNOT1 and CNOT4 on RNA half-lives were predominantly seen in protein coding messenger RNAs (Supplemental Figure S7B). To rule out changes in half-lives caused by wide-spread metabolic changes in cells, we examined the changes in half-life of histone mRNAs. Most histone mRNAs are not polyadenylated and would be insensitive to inactivation of CCR4-NOT (Marzluff et al. 2008). Indeed, depletion of either CNOT1 or CNOT4 had minimal effect on the turnover of non-polyadenylated histone

mRNAs (Figures 5F, Supplemental Figure S7C-D). Interestingly, there are a few histone variant mRNAs that are polyadenylated (Marzluff et al. 2008), such as *H1.0*, and depleting CNOT1 or CNOT4 changed its stability similar to other mRNAs. Specifically, the half-life of this mRNA was increased in CNOT1-depleted cells and decreased in CNOT4-depleted cells (Supplemental Figure S7E). Finally, these results were validated by RT-qPCR analysis of specific messages (Supplemental Figure S8A-I).

Next, to address if the effects of CNOT1 and CNOT4 depletion on RNA half-life are a function of the steady state half-life of the RNA, we ranked RNAs based on their half-lives and sorted them into quartiles (Q1-Q4, each N ≈ 3950). Q1 represents highly unstable RNAs (median half-life in steady-state control conditions ~ 3.7 h) and Q4 represents highly stable RNAs (median half-life in steady-state control conditions ~ 45 h). Depletion of CNOT1 resulted in obvious increase in half-life in quartiles 1, 2 and 3, while surprisingly RNAs in Q4 showed significant decrease in half-life and highly unstable RNAs (Q1) showed highest increase in half-life (median increase in half-life ~3-fold) as compared to others (Supplemental Figure S9A-B). The destabilizing effect by depletion of CNOT4 was observed in all the quartiles, although highly stable RNAs in Q4 ($t_{1/2}$ > 22.8 h) showed a stronger decrease in half-lives (Supplemental Figure S9C). These findings were further corroborated by the observation that the steady-state half-life negatively correlated with changes in RNA half-life induced by CNOT1 depletion or CNOT4 depletion (Supplemental Figure S9B-C). These data overall suggested that highly unstable RNAs are the most sensitive targets for the degradation by CCR4-NOT complex. On the other hand, highly stable RNAs are least sensitive to CCR4-NOT complex, and this group of RNAs is most influenced by CNOT4.

Effects of depletion of CNOT1 and CNOT4 are influenced by codon optimality content

Codon optimality is an important feature that influences mRNA stability. Stable mRNAs tend to be enriched with optimal codons, while unstable mRNAs have more non-optimal codons (Forrest et al. 2020; Presnyak et al. 2015; Bae and Coller 2022; Wu et al. 2019). Codon optimality in an mRNA influences ribosome translocation rates during translation, which is sensed by CCR4-NOT complex (Buschauer et al. 2020; Absmeier et al. 2023). When ribosome encounters a non-optimal codon, the inability to fill the A-site with a cognate tRNA causes ribosome stalling and an empty E-site. The N-terminus of the Not5 subunit of Ccr4-Not complex fits into this site, which triggers mRNA degradation (Buschauer et al. 2020). We next asked if the sensitivity to subunit depletion on mRNA turnover correlated with codon optimality content of the message. As a codon optimality measure, we used previously published datasets of codon stability coefficients ['CSC', (Forrest et al. 2020)] and partial least squares score for codon optimality ['PLS', (Medina-Muñoz et al. 2021)]. First, we compared these optimality matrices with the half-lives we calculated under control (undepleted) conditions (Figures 6A, Supplemental Figure S10A). We observed a strong and highly significant correlation between codon optimality content and transcript half-lives, suggesting

that our measurements indeed supported the previously known relationship between codon content and mRNA half-lives (Forrest et al. 2020; Presnyak et al. 2015). We binned mRNAs into 'optimal' (optimality score > 0) and 'non-optimal' (optimality score < 0) groups. The median half-life of optimal mRNAs was indeed significantly higher than 'All', while that of non-optimal mRNAs was significantly lower (Figures 6B, Supplemental Figure S10B). Further, we hypothesized that if CCR4-NOT regulates mRNA turnover depending upon codon optimality, the mRNAs enriched with non-optimal codons would be more affected by CNOT1 depletion. Since depletion of CNOT1 showed a global increase in mRNA half-lives, the changes were interpreted as 'less increased' or 'more increased' contexts. First, changes in mRNA half-life upon depletion of CNOT1, did correlate negatively to codon optimality content with high significance (Figures 6C, Supplemental Figure S10C). This suggested that the non-optimal mRNAs are more stabilized than their counterparts upon CNOT1 depletion. This was further corroborated by the finding that median increase in half-life for non-optimal mRNAs was significantly higher than all mRNAs, while that for optimal mRNAs was significantly lower (Figures 6D, orange data points, Supplemental Figure S10D). While overall, the trends are the same between CNOT1- and CNOT4 depleted cells in that the CSC or PLS scores negatively correlated with changes in half-life, comparison of the changes in half-lives CNOT4-depleted cells and codon optimality content revealed a surprising pattern (Figures 6C, purple data points, Supplemental Figure S10C). Because depletion of CNOT4 led to global decrease in half-life (negative values), versus an increase in CNOT1 depleted cells, we might have expected the opposite correlation. Those with higher CSC scores or PLS scores (optimal mRNAs with higher stability) would trend towards lesser decrease in half-lives and those with lower CSC or PLS score (non-optimal mRNAs with lower stability) would trend towards higher decrease in half-lives. The data in fact suggest that the non-optimal mRNAs are less destabilized (relatively lesser decrease in stability) upon CNOT4 depletion. Indeed, the median decrease in half-life for non-optimal mRNAs was significantly lower than 'All', while that for optimal mRNAs was significantly higher than 'All' (Figures 6E, Supplemental Figure S10E). The precise mechanism behind the effects of CNOT4-depletion on RNA half-life warrants further investigation and is speculated upon in the discussion section.

Depletion of CNOT1 and CNOT4 leads to wide-spread increase in nascent transcription

Depletion of CNOT4 increased turnover rates of RNAs transcriptome-wide, but the steady-state levels did not change significantly (Figures 4, 5). These findings suggested that synthesis is increased to buffer changes in turnover (Timmers and Tora 2018). Studies on yeast Ccr4-Not reveals that it regulates transcription by promoting elongation and/or affecting TBP activity (Badarinarayana et al. 2000; Denis et al. 2001; Reese 2013), but it is still unclear if human CCR4-NOT regulates gene expression at the level of transcription. To address this, we performed transient transcriptome sequencing (TT-seq) by 4-thioU labeling (Schwalb et al. 2016; Gregersen et al. 2020). DLD-

1^{TIR1+}, $CNOT1^{AID}$ and $CNOT4^{AID}$ cells were treated with auxin for 2 and 8 h, followed by a brief 15-minute pulse of 4-thioU labeling. Labeled RNAs were then captured and sequenced followed by differential expression analysis by normalizing the data using a spike-in control (*S. pombe* 4-thioU labeled RNA). Each experimental condition had 2 biological replicates which showed high reproducibility (R> 0.99, Supplemental Table S2). Interestingly, depleting CNOT1 or CNOT4 resulted in a significant increase in nascent transcription across the genome after 2 h of depletion (Figure 7A and Supplemental Figure S11B). Depletion of the protein takes at least 1hr (Figure 1 and S1), so this is an immediate response. The analysis revealed hundreds to thousands of genes differentially transcribed (DTGs) under depletion conditions (Figure 7A and Supplemental Figure S11C-F), of which ≥ 85% of the genes showed enhanced transcription (> 1.5 FC, p^{adj} < 0.01 cutoff) and these genes mainly encoded protein coding mRNA transcripts (~90% of DTGs, (Supplemental Figure S11G-I). Extending the depletion time to 8 h showed that the number of DTGs did not change much when CNOT4 was depleted, but the number of genes in CNOT1-depleted cells continued to increase through to 8 h of protein depletion. Whether or not secondary effects contributed to the increase in DTGs at 8 h is uncertain, but depleting CNOT1 changed the steady state levels of mRNA of multiple transcription factors (Supplemental Figure S6 and see discussion). These data suggest that depletion of CNOT1 and CNOT4 leads to rapid and widespread increase in transcription. Furthermore, since depleting CNOT4 and CNOT1 had opposite effects on mRNA turnover, this suggests that the effects on transcription does not directly result from changes in mRNA decay.

CNOT1 and CNOT4 regulate transcription of the KRAB-Zinc finger repressor family genes

K-means clustering of changes transcription showed a widespread increase in transcription in CNOT1- and CNOT4-depleted cells (Figure 7A, clusters 1 and 2). Although there was a global increase in transcription, the genes comprising cluster 3 were notably reduced (Figure 7A, cluster 3). GO analysis of genes in cluster 3 returned the term 'DNA binding transcription factor activity' as overrepresented (Supplemental Figure 12A. 143 genes, 2.1x enrichment, 2.3E-14 FDR). Closer inspection of these transcription factors revealed that most (109/143) were KRAB-ZNFs genes (Kruppel associated box containing Zinc finger protein coding, referred to as KZNFs hereafter), which function in gene repression (Figure 7B, Supplemental Figure S12B-C). To gain more insights into this novel finding, we examined the data in another way. We clustered the transcriptional changes of all ZNF genes whose data were available in this study (N = 642). The majority of the ZNF genes showed a widespread increase in transcription upon depletion of CNOT1 and CNOT4, like the rest of the genome (Figure 7C, cluster C, N = 559). However, the group of ZNFs that showed reduced transcription (Figure 7C, clusters A and B, cumulative N = 83) were greatly enriched for KRAB-domain containing ZNF genes (Supplemental Figure S12C).

Since KZFPs are highly abundant and bind throughout the genome, we speculated that the wide-spread increase in nascent transcription observed in depleted cells is caused by reduced KZFP repression. We analyzed published Chip-exo data of genome-wide binding of KZFPs (Imbeault et al. 2017). We specifically looked at KZNFs whose transcription is repressed in depleted cells (KZNFs in cluster 3, Figure 7A). We observed a very strong overlap between DTGs and genes having at least 1 KZFP binding peak within or ±1KB of the gene (Figure 7D). ~90% of the DTGs had at least one KZFP associated with them. The binding peaks of the KZFPs whose expression were reduced were more enriched at genes whose transcription increased than those whose transcription was repressed upon CNOT1 or CNOT4 depletion (Figure 7E). This strong association suggests that the wide-spread increase in transcription is mediated by reduced KZFP expression.

CNOT1 and CNOT4 depletion results increased transcription of repeat elements, particularly LINEs.

KZFPs are the largest family of transcriptional repressors (Lupo et al. 2013), whose genes cluster on chromosome 19, *chr19* (Shannon et al. 1996; Vogel et al. 2006). Thus, we looked at the chromosomal location of KZNFs regulated by CNOT1 or CNOT4. The analysis indeed revealed that transcription of KZNFs present on chr19, in particular, is under the control of CCR4-NOT (Figure 8A). KZFPs on Chr19 have been shown to have expanded and evolutionary diversified alongside the rise of novel endogenous retroelements, and it has been proposed that there exists an evolutionary arms race between the endogenous retroelements and KZFPs (Jacobs et al. 2014). Loss of transcriptional repression of LINE1s has been followed by evolution of a new KZFP to execute their repression (Jacobs et al. 2014; Bruno et al. 2019; Imbeault et al. 2017; Lukic et al. 2014). KZFPs bind to and repress endogenous retroviral elements such as LINEs and repress protein coding genes by binding to promoters and ancient LTRs adjacent to genes (de Tribolet-Hardy et al. 2023; Rosspopoff and Trono 2023; Fasching et al. 2015; Ito et al. 2020; Pontis et al. 2022; Wolf et al. 2020; Lukic et al. 2014). To test if depletion of CNOT1 and CNOT4 leads to de-repression of repetitive elements, we re-mapped the TT-seq data using the Allo tool, which was recently developed to efficiently allocate multi-mapped reads with higher accuracy to locations within the genome (Morrissey et al. 2024). The data revealed that the expression of L1 LINE retrotransposons (LINEs) was in fact activated, along with the transcription of other repeat elements including some SINEs and LTRs of endogenous retroviruses (Figure 8B, C). We then analyzed the expression of LINEs detected in our dataset (N = 15611). There was a very noteworthy increase in LINEs transcription within 2 h of depleting CNOT1 or CNOT4 (Figure 8D, clusters 1 and 2, ~77% of all LINEs analyzed), which coincided with the repression of KZNFs genes (Figure 7C, clusters A and B). At 8 h of CNOT1 and CNOT4 depletion, the global de-repression of LINEs expression was still observed (Figure 8E, cluster 2 and 4), but there was a subset of LINEs that showed repression when CNOT1 was depleted (cluster 1). Partial recovery of LINEs suppression could be partly explained by the fact that depletion of CNOT1 for 8 h increased steady-state

levels of some KZNF mRNAs due to reduced mRNA decay, re-establishing repression (Figure 5 and data not shown). LINEs can impact the expression of adjacent genes by inhibiting transcription through heterochromatin formation or by promoting transcription by affecting promoter strength, acting as an enhancer, or providing an alternate promotor and transcriptional start site (TSS) (Elbarbary et al. 2016; Mätlik et al. 2006; Speek 2001). To investigate if the genome-wide effects on transcription we observed in CNOT1- and CNOT4-depletd cells are indeed a consequence of strong changes in LINE expression, we correlated the changes in expression of KZFP-bound LINEs with the change in expression of the adjacent genes. We focused on those KZFPs which have the highest number of peaks genome-wide, and are repressed in CCR4-NOT depleted cells (same set of KZFPs were analyzed in Figure 7D-E). The analysis revealed a very strong and highly significant correlation between the transcriptional changes of LINEs and their adjacent genes (Figure 8F-G). Similar correlations were observed with other transposable repeat elements including SINEs, LTRs etc. (Spearman's rho > 0.35, p-value < 3.02E-42, data not shown). Together, these findings suggest a novel mechanism by which CCR4-NOT regulates transcription genome-wide, by regulating KZFPs to silence repeat elements and adjacent genes.

Discussion

Despite several years of work, the functions of human CCR4-NOT complex are not fully understood, especially its role in transcription. Here we employed rapid auxin inducible degron (AID) strategy to examine the functions of the hCCR4-NOT complex in cell culture. Furthermore, a conditional depletion strategy is necessary because deletion CNOT1 of is considered lethal, and our analysis has confirmed that cells arrest and ultimately die in the absence of CNOT1 (Supplemental Figure S2A). Furthermore, we addressed the effects of hCCR4-NOT depletion on ongoing transcription by TT-seq, which led to the remarkable observations that CCR4-NOT globally represses ongoing transcription and identify the complex as a novel silencer of transposon activation.

One outcome from our studies was to confirm that even though CNOT4 does not co-purify with the complex using multiple methods [Figure 2 and (Lau et al. 2009)] it associates with the complex in vivo, based on proximity labeling (BioID). Others have noted that CNOT4 is labeled other CCR4-NOT subunits using the original BirA biotin ligase (Youn et al. 2018). Although both subunits associate with the complex and associate with a similar collection of proteins, depleting CNOT1 and CNOT4 exhibited distinct phenotypes. Depleting CNOT1 resulted in the disintegration of the complex, inhibition of cell growth, G1/S arrest and global increase in steady state RNA levels; depletion of CNOT4 resulted in none of these phenotypes. More striking is the effects on mRNA half-lives. As anticipated, our RNA half-life measurements revealed an overall increase in RNA stability in CNOT1-depleted cells, consistent with multiple studies showing that depleting CNOT1 or the deadenylase subunits CNOT6/6L or CNOT7/8 extended mRNA half-life globally (Gillen et al. 2021; Mostafa et al. 2020). Specifically, Gillen et al showed

that siRNA depletion of CNOT1 resulted in increased global stability of mRNAs, and our data correlated quite well with theirs (R = 0.45, p<4.8e-235). That study found that mRNAs enriched for G/C-ending codons were especially sensitive to CNOT1 depletion. However, we did not find preference in stabilization of with G/C terminal codons (not shown). Whether this is difference is cell type specific or explained by our rapid, acute depletion, versus the longer-term RNAi partial reduction in CNOT1 remains to be determined.

Until now, the effects of CNOT4 depletion on gene expression has not been reported. In contrast to what was observed in CNOT1-depleted cells, depleting CNOT4 had the opposite effect on mRNA decay. Depletion of CNOT4 resulted in the quite remarkable global increase in RNA decay rates (Figure 5). Depletion of CNOT4 destabilized a majority of the RNAs, but its effect was more pronounced on highly stable mRNAs with higher codon optimality content (Figure 6) suggesting that these RNAs have stronger dependency on CNOT4 and CNOT4 differentially influences subgroups of RNAs. RNF219 is another RING domain-containing E3 ligase that associates with CCR4-NOT and, like what we found for CNOT4, its depletion accelerated mRNA decay (Poetz et al. 2021). RNF219 binds to the CNOT9 module, once again, like CNOT4. This begs the question if different subcomplexes exist, one with CNOT4 and another containing RNF219. The authors of the prior study speculated that RNF219 globally attenuates deadenylase activity by impeding the access of poly-A RNA to the catalytic module or by reducing the catalytic activity of deadenylases. The function of CNOT4 can be envisaged in a similar context. However, it is also possible that CNOT4 may regulate the partitioning of mRNAs into distinct pools in the cell. For example, yeast Ccr4-Not regulates the solubility of mRNAs, which impacts their degradation. The solubility of mRNAs correlates with the codon optimality and that co-translational decay is inversely regulated by Not1 and Not4 (Allen et al. 2023). Although a similar mechanism is yet to be established in mammalian cells, it is plausible that depletion of CNOT4 leads to changes in the solubility or partitioning of mRNAs into distinct pools, which affect their decay rate.

Although depleting CNOT4 resulted in rapid turnover, there was minimal change in steady-state RNA levels (Figure 4). Steady state RNA levels reflect a balance between two opposing RNA synthesis and decay. In eukaryotic cells, these two processes are connected in such a way that a change in one parameter results in an opposing change in the other to maintain steady-state levels closer to the normal amount, a phenomenon called as transcript buffering (Shalem et al. 2008, 2011; Timmers and Tora 2018). This involves many key players in RNA synthesis (Pol II, TFIID, TFIIH and SAGA) and in RNA decay (Xrn1, Lsm-Pat1, Ccr4-Not complex, and the exosome complex). In the CNOT4 cells, it appears buffering is underway, because increased turnover was buffered by increased synthesis or vice versa (see below). Interestingly, this was not the case for CNOT1 depleted cells (Figure 5 and 7A). Depletion of CNOT1 essentially causes the loss of the CCR4-NOT complex, Figure 2), and the major

deadenylase (Supplemental Figure S3). Since decay is strongly impaired, the machinery needed to respond to the increased transcription is inactive; thus, cell lose the capacity to buffer the change in synthesis. In contrast, depleting CNOT4 had no effect on the integrity of the CCR4-NOT complex (Figure 2) enabling buffering response to the accelerated RNA-decay by increased nascent transcription.

CCR4-NOT has been more thoroughly characterized in yeast, where it was initially defined as a transcription regulator [reviewed in (Chalabi Hagkarim and Grand 2020; Miller and Reese 2012; Collart 2016)]. The function of human CCR4-NOT in transcription is largely unknown and it was unclear if the transcription functions identified in yeast are conserved. Remarkably, we found that depletion of CNOT1 or CNOT4 caused moderately widespread increase in transcription, which was evident as early as 2 h of depletion (Figure 7A and Supplemental Figure S11). It is noteworthy that the other phenotypes resulting from CNOT1 or CNOT4 depletion are very different, except for its effect on genome-wide transcription. The fast response to depletion (2 h) on transcription suggests a direct effect and a decoupling from the effect on mRNA decay. A close examination of the time course of deletion revealed discernable differences on transcription. The number of differentially transcribed genes (DTGs) did not change much 8 h versus 2 h of CNOT4 depletion (~1200 at 2 h and ~1600 at 8 h; with > 85% genes showing increased transcription). On the other hand, the number of DTGs in CNOT1-depleted cells increased from ~800 at 2 h to ~6500 at 8 h of depletion. Why the effects on transcription upon depletion of these factors differ is unclear. One speculation is since depletion of CNOT1 results in both increased transcription and decreased decay, there is global increase in steady-state RNA levels including those coding for transcriptional regulators. This might lead to increased levels of transcription regulators which would contribute to further increase in nascent transcription at 8 h. On the contrary, the increased changes in transcription are buffered by increased decay in CNOT4-depleted cells resulting in no significant change in steady state levels upon 8 h of depletion.

Depleting CNOT1 or CNOT4 repressed transcription of genes coding KZFPs, specifically those located on chromosome-19. KZFPs are the largest family of transcriptional repressors in vertebrates. The human genome has ~350 KZNFs; and ~200 of these genes are positioned within six clusters on chromosome 19 (Lukic et al. 2014). Recent studies revealed that KZFP function in transcriptional silencing by binding to and repressing transposable elements (TEs), mainly retrotransposons (Ecco et al. 2017), such as LINEs. LINEs are a class of non-long terminal repeat (LTR) retrotransposons that have enormous potential for regulating chromatin structure and transcription of adjacent genes (Elbarbary et al. 2016; Chuong et al. 2017; Lykoskoufis et al. 2024; Liu et al. 2018; Brattås et al. 2017; Osipovich et al. 2023; Ecco et al. 2016; Guio et al. 2018; Gebrie 2023). It is noteworthy that several other KZFP don't bind to TEs, but have other genomic targets such as gene promoters or gene body (Imbeault et al. 2017; Frietze et al. 2010). Furthermore, the LTRs of ancient TEs that have lost their coding capacity have been shown to

regulate adjacent genes through a process of co-option (Kunarso et al. 2010; Macfarlan et al. 2012; Chuong et al. 2016). It is likely that Ccr4-Not tunes over transcription levels in cells and suppresses spurious transcription by maintaining KZFP expression (Figure 7 and data not shown). A strong correlation was observed between changes in transcription of transposable elements (LINEs, SINE and LTRs) and their adjacent genes (Figure 8F-G) suggest the rTE repression and global gene expression are linked. The precise mechanism behind how CCR4-NOT regulates KZNF expression is yet to be elucidated, and is beyond the scope of this work, but one possibility is that CCR4-NOT directly targets KZNFs genes to drive their transcription. Alternatively, CCR4-NOT targets transcription factors that control KZFPs expression, possibly by rapid turnover via CNOT4-dependent ubiquitination and protein degradation.

LINEs have been implicated in several human diseases like Hemophilia A and B, Duchenne muscular dystrophy, Coffin-Lowry syndrome, colon cancer, β-thalassemia etc., X-linked retinitis pigmentosa (Hancks and Kazazian 2012). Specifically, spurious activation of LINEs has deleterious effects on the cellular function as well as genomic stability, which contributes to the manifestation of a disease (Bhat et al. 2022). LINEs cause gene disruption and significant genomic alterations like duplications, inversions, deletions (Gasior et al. 2006; Lin et al. 2009).Yeast and human Ccr4-not play important roles in maintain genomic integrity, including the repair of DNA (Jiang et al. 2019; Traven et al. 2005). The mRNA deadenylase activity of Ccr4-Not is required for DNA damage responses under genotoxic stress. Recently, it was shown that partial knockdown of CNOT1 by siRNA transfection resulted in increased bulk transcription, as measure by 5-ethynyl uridine (EU) incorporation and microscopy of stained cells (Hagkarim et al. 2023). Interestingly, increased R-loop (RNA:DNA hybrids) formation and genome instability was also observed in the knockdown cells. R-loops are enriched in genomic regions with a higher abundance of L1 LINEs (Nadel et al. 2015; Abakir et al. 2020). Our finding that depletion of CNOT1 or CNOT4 leads to robust increase in LINE expression suggests that CCR4-NOT complex preserves genomic stability and integrity by suppressing widespread, spurious transcription. This is achieved by CCR4-NOT maintaining KZNF transcription that suppresses the expression of retrotransposable elements including LINEs; thus CCR4-NOT's function in transcription and genome stability is mediated through the KZFP class of transcription repressors.

Methods

Cell lines

DLD-1 cells (ATCC CCL-221) were purchased from ATCC and DLD-1^{TIR1+} cells were a kind gift from Dr. Mary Dasso at National Institutes of Health, USA. Cells were maintained in complete media [Dulbecco's Modified Eagle Medium

(DMEM) with 10% Fetal Bovine Serum, 1X glutamax and 1X Penicillin and Streptomycin] in 5% CO2 atmosphere at 37 °C in a humidified incubator.

Plasmid construction

All the primers and plasmids used in this study are listed in Supplementary Table S3. The AID knock-in vectors (donor plasmids) were generated using In-Fusion cloning (Takarabio) generated by PCR. To generate the vector backbone, pVA181 plasmid (see Supplementary Table S3) was digested with EcoRV and NotI and used in *in-fusion* assembly. Clones were screened with restriction enzymes and sequencing. The plasmids for Turbo ID and miniTurboID were generated using In-Fusion cloning as described for mini-AID knock-in vectors, except the sequence coding for mini-AID was replaced with either mini-Turbo-ID; *mTID* Turbo-ID (Branon et al. 2018). The sequences coding for mTID and TID were synthesized as gene-blocks from IDT. Plasmid sequences available upon request.

CRISPR-Cas9 gene editing

A plasmid to produce CNOT1 gRNA or CNOT4 gRNA was made from pX330 (gift from Dr. Mary Dasso, National Institutes of Health) by inserting a double-stranded olionucleotide corresponding to CNOT1 or CNOT4 gRNA into the BbsI site of the vector. CRISPR mediated mini-AID (referred to AID henceforth) was done as described (Aksenova et al. 2022) with some modification. Cells were seeded in 35 mm dishes so as to reach 50% confluency at the time of transfection. Media were changed to Opti-MEM with 10% FCS. 3 µg of plasmid DNA (1.5 µg of gRNA plasmid + 1.5 µg of donor plasmid) was mixed with 9 µl of Viafect in 300 µl of Opti-MEM. The mixture was incubated at room temperature for 15 min. and was added to cells. 72 hrs. post-transfection, cells were trypsinized, transferred to a 100 mm dish and were cultured in selective complete media with 200 µg/ml Hygromycin-B for 2 weeks. The media containing dead cells were replaced with PBS and colonies were transferred to the wells of a 24-well plate containing trypsin solution, incubated at 37 °C for 15-20 minutes to dissociate cells, followed by addition of fresh complete media with 200 µg/ml Hygromycin. Cells were cultured till formation of monolayer. The cells were cultured in Hygromycin media for one additional passage following which they were cultured in complete media without Hygromycin. Generation of TID/mTID knock-in cell lines was carried out as described for AID tagged cell lines except transfections were done using Lipofectamine3000 using manufacturer's instructions. Potential clones were screen by PCR screening of gDNA and by western blotting for CNOT1 and CNOT4 (see reagent table and Supplementary Table S3. Details on western blotting and PCR are described in Supplementary Methods.

Bio-ID

Cells (Parental DLD-1, CNOT1^{mTID}, CNOT4^{TID}) were seeded in 100 mm dishes for 24 hrs. At ~70% confluency old media were replaced with pre-warmed media containing 100 mM biotin. After one hour, media were decanted and cells were washed with ice-cold PBS, collected and lysed in RIPA buffer (50 mM Tris pH 8, 150 mM NaCl, 0.1% SDS, 0.5% sodium deoxycholate, 1% Triton X-100, Protease inhibitors and 1 mM PMSF) on ice for 20 minutes. The lysates were sonicated on Bioruptor™ UCD-200 in ice-water slurry (4 pulses of 30 sec on and 30 sec off on 'high' setting). The lysates were clarified by centrifugation at 13,000 rpm at 4 °C for 10 minutes. The supernatant was collected and protein estimation was done using BCA protein estimation kit. To enrich biotinylated proteins, Pierce™ Streptavidin Magnetic Beads (pre-equilibrated with RIPA buffer) were incubated with 1 mg of lysates overnight. The beads were captured on magnet and were subsequently washed in the following order (each wash was 1 ml) - twice with RIPA buffer, once with 1 M KCl, once with 0.1 M Na2CO3, once with 2 M urea in 10 mM Tris-HCl (pH 8.0), twice with RIPA buffer and finally once with 10 mM Tris-HCL, pH 8, 1 mM EDTA. The beads with enriched biotinylated proteins were frozen at -80 °C till further processing. For on-beads tryptic digestion, the beads were washed once with 0.4 ml 50 mM Tris pH 8.5, 2M urea, 1 mM DTT, followed by resuspension in 75 µl 50 mM Tris (pH 8.5), 1 M Urea, 1 mM DTT, and 1 µg of Promega Trypsin Gold Trypsin (0.5 mg/ml prepared in 50 mM acetic acid). The reaction was incubated at 4 hrs. at 37 °C with shaking. The supernatants were collected in fresh tubes and the beads were washed twice with 50 µl 50 mM Tris (pH 8.5), 1 M urea, 1 mM DTT and the washes were pooled with the original elution. DTT was added to a final concentration of 5 mM followed by incubation at 37 °C for 1 hr. Iodoacetamide was added to this to a final concentration of 10 mM and the reaction was incubated in the dark at room temperature for 30 minutes. An additional 0.5 µg trypsin was added and samples were digested overnight at 37 °C with shaking. The peptides were purified on C18 tips (Pierce-Thermofisher) after acidification with trifluoroacetic acid (TFA) to 0.5% using the manufacturers recommendations. The eluted peptides were dried down and frozen at -20 °C until TMT labelling. The peptides were resuspended in 50 µl 0.1M TEAB buffer followed by addition of TMTpro 16plex reagents and incubated at room temperature for 60 min. The reaction was quenched with hydroxylamine, dried down and repurified on reverse phase tips prior to loading onto Nano-flow Liquid Chromatography (Thermo Easy-nLC 1200). The peptides were loaded on an Acclaim PepMap100 trapping column (75 mm × 2 cm, C18, 5 mm, 100 Å, Thermo), and separated on an Acclaim PepMap RSLC column (50 mm × 15 cm, C18, 2 mm, 100 Å, Thermo) at a flow rate of 300 nL/min in the following gradient of mobile phase B (80% ACN in 0.1% aqueous FA): 5% - 50% B in 210 min, 50% - 90% B in 30 min. A Thermo Orbitrap Eclipse mass spectrometer was operated in a data dependent mode using a method based on the TMT MS2 template. The resulting mass spectra were processed using Proteome Discoverer 3.1 software.

Chromatographic separation of hCCR4-NOT complex

CNOT1^{AID} or CNOT4^{AID} cells from 100 mm dishes were treated ± 1 mM auxin for 4 hrs. Cells were collected by scrapping off in ice-cold PBS and lysed in hypotonic lysis buffer (10 mM HEPES, 1.5 mM MgCl2, 10 mM NaCl, 0.2 mM PMSF, 0.5 mM DTT. 1 µg/ml leupeptin, 1 µg/ml aprotinin and 1 µg/ml pepstatin A. 1mM benzamidine-HCL) on ice for 10 min, homogenized and nuclei were pelleted by spinning at 4000 rpm [JS-4.2 rotor], 4 °C, 15 minutes. The supernatant was added with 0.11 volume of 10X cytoplasmic extract buffer (0.3 M HEPES, 1.4 M NaCl, 0.03 M $MgCl_2$, protease inhibitors. 0.2 mM PMSF, 0.5 mM DTT) and Benzonase (1 µl per 600 µl extract), incubated on ice 30 minutes. The lysate was further spun down at 13,000 rpm for 20 min, at 4 °C. The supernatant was dialyzed at 4 °C in dialysis buffer (20 mM HEPES/NaOH, 150 mM NaCl, 10 µM $ZnCl_2$, 1mM DTT, 10% glycerol, 0.5 mM PMSF, 0.2 µg/ml leupeptin, 0.2 µg/ml aprotinin and 0.5 µg/ml pepstatin A, 1 mM benzamidine-HCL) for 4 hours, spun at 14,000 rpm for 10 min at 4 °C and the supernatant was concentrated using Vivaspin concentrator (20 kDa cutoff) to 5-6 mg/ml protein. Two to three mg of lysate was loaded onto a Superose 6 size exclusion chromatography column, run on ÄKTA pure™ chromatography system (GE Life sciences) in chromatography buffer (20 mM HEPES/NaOH, 150 mM NaCl). Fractions were concentrated by TCA precipitation and analyzed by western blotting.

RNA extraction

Following the treatment with ±1mM auxin for desired time, media were decanted and the cells were lysed directly in 1 ml Trizol. The cells were resuspended thoroughly by pipetting up and down several times and were incubated at room temperature for 5 minutes. 0.2 ml chloroform was added per 1 ml of Trizol. The tubes were capped and shaken vigorously by hand for 15 seconds and then were incubated at room temperature for 2-3 minutes. The mixture was then centrifuged at > 12,000 xg for 15 min at 4 °C, the aqueous phase was collected in a separate tube followed by addition of equal volume of 100% ethanol. The RNA was cleaned up using Ambion RNA PureLink Kit according to manufacturer's instructions and eluted in 100 µl RNase-free water.

DNase treatment, tape station, cDNA synthesis and RT-qPCR

10 µg of total RNA was treated with Turbo DNase (TURBO DNA-free™ Kit) for 30 minutes at 37 °C. 10 µl of DNase inactivation agent was added to the reaction followed by incubation at room temperature for 5 minutes. The tubes were flicked 2–3 times during the incubation period to keep the DNase Inactivation Reagent suspended. The reaction was centrifuged at 10,000 × g for 90 seconds and supernatant was transferred in a new tube. The integrity of RNA was assessed by Agilent TapeStation-4150 at the Genomics Core Facility, Penn State University, USA. RNA samples with RIN score > 9.5 were used for further work. 1 µg of DNase digested RNA was used to make cDNA using RevertAid First Strand cDNA Synthesis Kit according to manufacturer's instructions using Oligo (dT)18 primer and Random Hexamer primer (mixed 1:1). The cDNA product was directly used in PCR applications or stored at -

20 °C until used. RT-qPCR was performed using PerfeCTa SYBR® Green SuperMix (Quantabio). Two dilutions of cDNA were used in RT-qPCR to ensure the linear range of amplification. For each condition at least 2 experimental replicates were used. The RT-qPCR was run on Agilent Real-time PCR machine (G8830A) and the data were analyzed using Agilent AriaMx and Microsoft excel.

RNA sequencing

Sequencing libraries for steady-state RNA-seq or triptolide RNA-seq to measure half-lives were generated using Illumina Stranded Total RNA Prep with Ribo-Zero Plus according to manufacturer's instructions. Briefly, 500 ng of Turbo DNase digested RNA was mixed with 2 µl of 1:200 diluted ERCC Spike-in mix (final volume 11 µl) which was subjected to the first step of library prep (i.e. probe hybridization). The sequencing libraries were analyzed on TapeStation-4150 at the Genomics Core Facility, Penn State University, USA and were quantified using NEBNext® Library Quant Kit for Illumina®. The libraries with multiple indices were pooled and treated with Illumina® Free Adapter Blocking Reagent according to manufacturer's instructions. Sequencing was carried out at Genomics Research Incubator, Penn State University, USA using NextSeq™1000/2000 P2 Reagents(100Cycles) on NextSeq 2000. FASTQ files were further processed as per the Bulk RNA-seq Data Standards and Processing Pipeline (https://www.encodeproject.org/), using STAR [(Dobin et al. 2013), version - STAR_2.5.1b_modified] and RSEM (RNA-Seq by Expectation-Maximization) tool. The reads were mapped to hg38 (GRCh38) using Gencode-v29 comprehensive gene set, predicted tRNA genes, and the ERCC spike-in controls (ThermoFisher Scientific). Read-counts for each gene generated by RSEM were used for differential expression analysis using DESeq2 (Love et al. 2014). Genes with a sum of ≥ 8 across both replicates and conditions were used in DESeq2. The expression data were normalized to ERCC spike in controls using estimateSizeFactors function in DESeq2. Genes showing ≥ 1.5-foldchange at padj < 0.01 were denoted as differentially expressed.

Transient transcriptome sequencing (TT-seq)

TT-seq libraries were generated as described previously (Gregersen et al. 2020). Briefly, cells (parental, CNOT1^{AID} and CNOT4^{AID}) were grown in 150 mm dishes to reach 70% confluency at the time of auxin treatment (2 hrs. or 8 hrs.). Cells were then labelled by addition of 4-Thiouridine (4TU, final concentration 500 µM) to the media for 15 minutes. All the work involving 4TU was performed under conditions of minimal direct light exposure. Media were discarded and cells were immediately lysed in Trizol. RNA extraction was carried out as described earlier. 200 µg of total RNA was mixed with 5 µg of spike in control (total RNA from *S. pombe* labelled with 4TU, described in Supplemental Methods) in a 250 µl reaction. RNA fragmentation was carried out by addition of 50 µl NaOH (1M) to this reaction (40 minutes on ice). RNA fragmentation was stopped by addition of 200 µl Tris (1M, ph 6.8). The

RNA was Phenol/Chloroform extracted and used for *in vitro* biotinylation using MTS-Biotin. RNA was heated at 65 °C for 10 minutes, quick-chilled on ice followed by addition of 1X biotin buffer and MTS-biotin (Biotium). Biotinylation was carried out in dark at room temperature for 40 minutes on a rotator and was followed by Phenol/Chloroform extraction to remove excess biotin. After heating at 65 °C and quick-chilled on ice, RNA was captured on Streptavidin beads (Dynabeads™ MyOne™ Streptavidin C1) at room temperature for 20 minutes. Beads were washed in wash buffer (100 mM Tris-HCl, pH 7.4, 1 M NaCl, 10 mM EDTA, and 0.1% Tween 20; prewarmed at 55 °C) 6 times followed by elution by incubating in 100 mM DTT (twice, 5 minutes each). The pooled eluates were precipitated with in presence of 0.5M NaCl and 0.2 mg/ml glycogen. RNA was estimated by Qubit RNA estimation kit.

Sequencing libraries were generated using Illumina Stranded Total RNA Prep with Ribo-Zero Plus according to manufacturer's instructions. 300 ng of RNA was heated at 65 °C and quick-chilled on ice followed by addition of EPH3 buffer (from library preparation kit) to get the buffer concentrations right for cDNA synthesis followed directly by first strand synthesis. Human (GRCh38) and *S. pombe* (ASM294v2) genomes were concatenated and reads were mapped to the combined genome using STAR aligner (version 2.7.11a). The raw counts of all reads mapping to the annotated region for each gene (i.e. intron + exon) were obtained using featureCounts. The gene read counts were transformed using variance stabilizing transformation (VST) in DESeq2 R-package. Both normalization and differential expression analysis were performed with the DESeq2 package. We used the *S. pombe* spike in read counts for normalization. Genes showing ≥ 1.5-foldchange at p-adj < 0.01 were denoted as differentially expressed.

Reagents

All the relevant reagents used in this study are listed in Supplementary Table S3.

Webtools and softwares

All the webtools and softwares used in this study are listed in Supplementary Table S3.

Data availability

All primary data obtained from RNA-Seq, RNA-seq (Triptolide) and TT-seq will be deposited at the Gene Expression Omnibus. Mass spectrometry data will be uploaded to the MassIVE database.

Author Contributions:

S.K. and C.S. performed the molecular and cell biology experiments. S.K.,A.M.,A.S.,B.G.,O.T.A., I.A. and S.M. performed gene mapping and bioinformatics analysis. C.A.K advised on library preparation and sequencing. A.A.

provided advice on performing gene editing and AID depletion. S.K. and J.C.R. conceived the experiments and wrote the paper.

Acknowledgements:

We thank members of Reese lab and that of the Center for Eukaryotic Gene Regulation (Penn State) for their helpful comments and suggestions. We would also like to thank Dr. Tatiana Laremore (Penn State Huck Proteomics and Mass Spectrometry Core Facility, RRID:SCR_024462) for mass spectrometric analyses; and several other core facilities at the Penn State University including Genomics (RRID:SCR_023645), Flow Cytometry (RRID:SCR_024460) and Genomics Research Incubator (RRID:SCR_024530). Mary Dasso (NIH) is recognized for providing DLD-1 Tir1 expressing cells and plasmids. Olive Geesman assisted in screening plasmid constructs for the BioiID experiments. This research was supported by funds from National Institutes of Health R35 GM136353 (J.C.R) and R35 GM144135 (S.M.).

References

Abakir A, Giles TC, Cristini A, Foster JM, Dai N, Starczak M, Rubio-Roldan A, Li M, Eleftheriou M, Crutchley J, et al. 2020. N6-methyladenosine regulates the stability of RNA:DNA hybrids in human cells. *Nat Genet* **52**: 48–55. http://www.ncbi.nlm.nih.gov/pubmed/31844323.

Absmeier E, Chandrasekaran V, O'Reilly FJ, Stowell JAW, Rappsilber J, Passmore LA. 2023. Specific recognition and ubiquitination of translating ribosomes by mammalian CCR4-NOT. *Nat Struct Mol Biol* **30**: 1314–1322. http://www.ncbi.nlm.nih.gov/pubmed/37653243.

Aksenova V, Arnaoutov A, Dasso M. 2022. Analysis of Nucleoporin Function Using Inducible Degron Techniques. *Methods Mol Biol* **2502**: 129–150. http://www.ncbi.nlm.nih.gov/pubmed/35412236.

Albert TK, Hanzawa H, Legtenberg YIA, de Ruwe MJ, van den Heuvel FAJ, Collart MA, Boelens R, Timmers HTM. 2002. Identification of a ubiquitin-protein ligase subunit within the CCR4-NOT transcription repressor complex. *EMBO J* **21**: 355–64. http://www.ncbi.nlm.nih.gov/pubmed/11823428.

Albert TK, Lemaire M, van Berkum NL, Gentz R, Collart MA, Timmers HT. 2000. Isolation and characterization of human orthologs of yeast CCR4-NOT complex subunits. *Nucleic Acids Res* **28**: 809–17. http://www.ncbi.nlm.nih.gov/pubmed/10637334.

Allen G, Weiss B, Panasenko OO, Huch S, Villanyi Z, Albert B, Dilg D, Zagatti M, Schaughency P, Liao SE, et al. 2023. Not1 and Not4 inversely determine mRNA solubility that sets the dynamics of co-translational events. *Genome Biol* **24**: 30. http://www.ncbi.nlm.nih.gov/pubmed/36803582.

Arango D, Sturgill D, Alhusaini N, Dillman AA, Sweet TJ, Hanson G, Hosogane M, Sinclair WR, Nanan KK, Mandler MD, et al. 2018. Acetylation of Cytidine in mRNA Promotes Translation Efficiency. *Cell* **175**: 1872-1886.e24. http://www.ncbi.nlm.nih.gov/pubmed/30449621.

Aslam A, Mittal S, Koch F, Andrau J-C, Winkler GS. 2009. The Ccr4-NOT deadenylase subunits CNOT7 and CNOT8 have overlapping roles and modulate cell proliferation. *Mol Biol Cell* **20**: 3840–50. http://www.ncbi.nlm.nih.gov/pubmed/19605561.

Badarinarayana V, Chiang YC, Denis CL. 2000. Functional interaction of CCR4-NOT proteins with TATAA-binding protein (TBP) and its associated factors in yeast. *Genetics* **155**: 1045–54. http://www.ncbi.nlm.nih.gov/pubmed/10880468.

Bae H, Coller J. 2022. Codon optimality-mediated mRNA degradation: Linking translational elongation to mRNA stability. *Mol Cell* **82**: 1467–1476. http://www.ncbi.nlm.nih.gov/pubmed/35452615.

Basquin J, Roudko V V, Rode M, Basquin C, Séraphin B, Conti E. 2012. Architecture of the nuclease module of the yeast Ccr4-not complex: the Not1-Caf1-Ccr4 interaction. *Mol Cell* **48**: 207–18. http://www.ncbi.nlm.nih.gov/pubmed/22959269.

Beck CR, Garcia-Perez JL, Badge RM, Moran J V. 2011. LINE-1 elements in structural variation and disease. *Annu Rev Genomics Hum Genet* **12**: 187–215. http://www.ncbi.nlm.nih.gov/pubmed/21801021.

Bhat A, Ghatage T, Bhan S, Lahane GP, Dhar A, Kumar R, Pandita RK, Bhat KM, Ramos KS, Pandita TK. 2022. Role of Transposable Elements in Genome Stability: Implications for Health and Disease. *Int J Mol Sci* **23**. http://www.ncbi.nlm.nih.gov/pubmed/35887150.

Branon TC, Bosch JA, Sanchez AD, Udeshi ND, Svinkina T, Carr SA, Feldman JL, Perrimon N, Ting AY. 2018. Efficient proximity labeling in living cells and organisms with TurboID. *Nat Biotechnol* **36**: 880–887. http://www.ncbi.nlm.nih.gov/pubmed/30125270.

Brattås PL, Jönsson ME, Fasching L, Nelander Wahlestedt J, Shahsavani M, Falk R, Falk A, Jern P, Parmar M, Jakobsson J. 2017. TRIM28 Controls a Gene Regulatory Network Based on Endogenous Retroviruses in Human Neural Progenitor Cells. *Cell Rep* **18**: 1–11. http://www.ncbi.nlm.nih.gov/pubmed/28052240.

Bruno M, Mahgoub M, Macfarlan TS. 2019. The Arms Race Between KRAB-Zinc Finger Proteins and Endogenous Retroelements and Its Impact on Mammals. *Annu Rev Genet* **53**: 393–416. http://www.ncbi.nlm.nih.gov/pubmed/31518518.

Buschauer R, Matsuo Y, Sugiyama T, Chen Y-H, Alhusaini N, Sweet T, Ikeuchi K, Cheng J, Matsuki Y, Nobuta R, et al. 2020. The Ccr4-Not complex monitors the translating ribosome for codon optimality. *Science* **368**. http://www.ncbi.nlm.nih.gov/pubmed/32299921.

Chalabi Hagkarim N, Grand RJ. 2020. The Regulatory Properties of the Ccr4-Not Complex. *Cells* **9**. http://www.ncbi.nlm.nih.gov/pubmed/33138308.

Chen C-YA, Shyu A-B. 2011. Mechanisms of deadenylation-dependent decay. *Wiley Interdiscip Rev RNA* **2**: 167–83. http://www.ncbi.nlm.nih.gov/pubmed/21957004.

Chen Y, Boland A, Kuzuoğlu-Öztürk D, Bawankar P, Loh B, Chang C-T, Weichenrieder O, Izaurralde E. 2014. A DDX6-CNOT1 complex and W-binding pockets in CNOT9 reveal direct links between miRNA target recognition and silencing. *Mol Cell* **54**: 737–50. http://www.ncbi.nlm.nih.gov/pubmed/24768540.

Chuong EB, Elde NC, Feschotte C. 2017. Regulatory activities of transposable elements: from conflicts to benefits. *Nat Rev Genet* **18**: 71–86. http://www.ncbi.nlm.nih.gov/pubmed/27867194.

Chuong EB, Elde NC, Feschotte C. 2016. Regulatory evolution of innate immunity through co-option of endogenous retroviruses. *Science* **351**: 1083–7. http://www.ncbi.nlm.nih.gov/pubmed/26941318.

Collart MA. 2016. The Ccr4-Not complex is a key regulator of eukaryotic gene expression. *Wiley Interdiscip Rev RNA* **7**: 438–54. http://www.ncbi.nlm.nih.gov/pubmed/26821858.

Collart MA. 2013. The Not4 RING E3 Ligase: A Relevant Player in Cotranslational Quality Control. *ISRN Mol Biol* **2013**: 548359. http://www.ncbi.nlm.nih.gov/pubmed/27335678.

Collart MA, Timmers HTM. 2004. The eukaryotic Ccr4-not complex: a regulatory platform integrating mRNA metabolism with cellular signaling pathways? *Prog Nucleic Acid Res Mol Biol* **77**: 289–322. http://www.ncbi.nlm.nih.gov/pubmed/15196896.

Dai X-X, Jiang Z-Y, Wu Y-W, Sha Q-Q, Liu Y, Ding J-Y, Xi W-D, Li J, Fan H-Y. 2021. CNOT6/6L-mediated mRNA degradation in ovarian granulosa cells is a key mechanism of gonadotropin-triggered follicle development. *Cell Rep* **37**: 110007. http://www.ncbi.nlm.nih.gov/pubmed/34788619.

de Tribolet-Hardy J, Thorball CW, Forey R, Planet E, Duc J, Coudray A, Khubieh B, Offner S, Pulver C, Fellay J, et al. 2023. Genetic features and genomic targets of human KRAB-zinc finger proteins. *Genome Res* **33**: 1409–1423. http://www.ncbi.nlm.nih.gov/pubmed/37730438.

Denis CL, Chiang YC, Cui Y, Chen J. 2001. Genetic evidence supports a role for the yeast CCR4-NOT complex in

transcriptional elongation. *Genetics* **158**: 627–34. http://www.ncbi.nlm.nih.gov/pubmed/11404327.

Dobin A, Davis CA, Schlesinger F, Drenkow J, Zaleski C, Jha S, Batut P, Chaisson M, Gingeras TR. 2013. STAR: ultrafast universal RNA-seq aligner. *Bioinformatics* **29**: 15–21. http://www.ncbi.nlm.nih.gov/pubmed/23104886.

Doidge R, Mittal S, Aslam A, Winkler GS. 2012. Deadenylation of cytoplasmic mRNA by the mammalian Ccr4-Not complex. *Biochem Soc Trans* **40**: 896–901. http://www.ncbi.nlm.nih.gov/pubmed/22817755.

Ecco G, Cassano M, Kauzlaric A, Duc J, Coluccio A, Offner S, Imbeault M, Rowe HM, Turelli P, Trono D. 2016. Transposable Elements and Their KRAB-ZFP Controllers Regulate Gene Expression in Adult Tissues. *Dev Cell* **36**: 611–23. http://www.ncbi.nlm.nih.gov/pubmed/27003935.

Ecco G, Imbeault M, Trono D. 2017. KRAB zinc finger proteins. *Development* **144**: 2719–2729. http://www.ncbi.nlm.nih.gov/pubmed/28765213.

Eisen TJ, Eichhorn SW, Subtelny AO, Lin KS, McGeary SE, Gupta S, Bartel DP. 2020. The Dynamics of Cytoplasmic mRNA Metabolism. *Mol Cell* **77**: 786-799.e10. http://www.ncbi.nlm.nih.gov/pubmed/31902669.

Elbarbary RA, Lucas BA, Maquat LE. 2016. Retrotransposons as regulators of gene expression. *Science* **351**: aac7247. http://www.ncbi.nlm.nih.gov/pubmed/26912865.

Fasching L, Kapopoulou A, Sachdeva R, Petri R, Jönsson ME, Männe C, Turelli P, Jern P, Cammas F, Trono D, et al. 2015. TRIM28 represses transcription of endogenous retroviruses in neural progenitor cells. *Cell Rep* **10**: 20–8. http://www.ncbi.nlm.nih.gov/pubmed/25543143.

Forrest ME, Pinkard O, Martin S, Sweet TJ, Hanson G, Coller J. 2020. Codon and amino acid content are associated with mRNA stability in mammalian cells. *PLoS One* **15**: e0228730. http://www.ncbi.nlm.nih.gov/pubmed/32053646.

Frietze S, Lan X, Jin VX, Farnham PJ. 2010. Genomic targets of the KRAB and SCAN domain-containing zinc finger protein 263. *J Biol Chem* **285**: 1393–403. http://www.ncbi.nlm.nih.gov/pubmed/19887448.

Gasior SL, Wakeman TP, Xu B, Deininger PL. 2006. The human LINE-1 retrotransposon creates DNA double-strand breaks. *J Mol Biol* **357**: 1383–93. http://www.ncbi.nlm.nih.gov/pubmed/16490214.

Gebrie A. 2023. Transposable elements as essential elements in the control of gene expression. *Mob DNA* **14**: 9. http://www.ncbi.nlm.nih.gov/pubmed/37596675.

Gillen SL, Giacomelli C, Hodge K, Zanivan S, Bushell M, Wilczynska A. 2021. Differential regulation of mRNA fate by the human Ccr4-Not complex is driven by coding sequence composition and mRNA localization. *Genome Biol* **22**: 284. http://www.ncbi.nlm.nih.gov/pubmed/34615539.

Graham T, Boissinot S. 2006. The genomic distribution of L1 elements: the role of insertion bias and natural selection. *J Biomed Biotechnol* **2006**: 75327. http://www.ncbi.nlm.nih.gov/pubmed/16877820.

Gregersen LH, Mitter R, Svejstrup JQ. 2020. Using TTchem-seq for profiling nascent transcription and measuring transcript elongation. *Nat Protoc* **15**: 604–627. http://www.ncbi.nlm.nih.gov/pubmed/31915390.

Guio L, Vieira C, González J. 2018. Stress affects the epigenetic marks added by natural transposable element insertions in Drosophila melanogaster. *Sci Rep* **8**: 12197. http://www.ncbi.nlm.nih.gov/pubmed/30111890.

Hagkarim NC, Hajkarim MC, Suzuki T, Fujiwara T, Winkler GS, Stewart GS, Grand RJ. 2023. Disruption of the Mammalian Ccr4-Not Complex Contributes to Transcription-Mediated Genome Instability. *Cells* **12**. http://www.ncbi.nlm.nih.gov/pubmed/37508532.

Hancks DC, Kazazian HH. 2012. Active human retrotransposons: variation and disease. *Curr Opin Genet Dev* **22**: 191–203. http://www.ncbi.nlm.nih.gov/pubmed/22406018.

Imbeault M, Helleboid P-Y, Trono D. 2017. KRAB zinc-finger proteins contribute to the evolution of gene regulatory networks. *Nature* **543**: 550–554. http://www.ncbi.nlm.nih.gov/pubmed/28273063.

Inada T, Makino S. 2014. Novel roles of the multi-functional CCR4-NOT complex in post-transcriptional regulation. *Front Genet* **5**: 135. http://www.ncbi.nlm.nih.gov/pubmed/24904636.

Ito J, Kimura I, Soper A, Coudray A, Koyanagi Y, Nakaoka H, Inoue I, Turelli P, Trono D, Sato K. 2020. Endogenous retroviruses drive KRAB zinc-finger protein family expression for tumor suppression. *Sci Adv* **6**. http://www.ncbi.nlm.nih.gov/pubmed/33087347.

Ito K, Takahashi A, Morita M, Suzuki T, Yamamoto T. 2011. The role of the CNOT1 subunit of the CCR4-NOT complex in mRNA deadenylation and cell viability. *Protein Cell* **2**: 755–63. http://www.ncbi.nlm.nih.gov/pubmed/21976065.

Jacobs FMJ, Greenberg D, Nguyen N, Haeussler M, Ewing AD, Katzman S, Paten B, Salama SR, Haussler D. 2014. An evolutionary arms race between KRAB zinc-finger genes ZNF91/93 and SVA/L1 retrotransposons. *Nature* **516**: 242–5. http://www.ncbi.nlm.nih.gov/pubmed/25274305.

Jiang H, Wolgast M, Beebe LM, Reese JC. 2019. Ccr4-Not maintains genomic integrity by controlling the

ubiquitylation and degradation of arrested RNAPII. *Genes Dev* **33**: 705–717. http://www.ncbi.nlm.nih.gov/pubmed/30948432.

Keskeny C, Raisch T, Sgromo A, Igreja C, Bhandari D, Weichenrieder O, Izaurralde E. 2019. A conserved CAF40-binding motif in metazoan NOT4 mediates association with the CCR4-NOT complex. *Genes Dev* **33**: 236–252. http://www.ncbi.nlm.nih.gov/pubmed/30692204.

Kohlrausch FB, Berteli TS, Wang F, Navarro PA, Keefe DL. 2022. Control of LINE-1 Expression Maintains Genome Integrity in Germline and Early Embryo Development. *Reprod Sci* **29**: 328–340. http://www.ncbi.nlm.nih.gov/pubmed/33481218.

Kunarso G, Chia N-Y, Jeyakani J, Hwang C, Lu X, Chan Y-S, Ng H-H, Bourque G. 2010. Transposable elements have rewired the core regulatory network of human embryonic stem cells. *Nat Genet* **42**: 631–4. http://www.ncbi.nlm.nih.gov/pubmed/20526341.

Lander ES, Linton LM, Birren B, Nusbaum C, Zody MC, Baldwin J, Devon K, Dewar K, Doyle M, FitzHugh W, et al. 2001. Initial sequencing and analysis of the human genome. *Nature* **409**: 860–921. http://www.ncbi.nlm.nih.gov/pubmed/11237011.

Lau N-C, Kolkman A, van Schaik FMA, Mulder KW, Pijnappel WWMP, Heck AJR, Timmers HTM. 2009. Human Ccr4-Not complexes contain variable deadenylase subunits. *Biochem J* **422**: 443–53. http://www.ncbi.nlm.nih.gov/pubmed/19558367.

Lin C, Yang L, Tanasa B, Hutt K, Ju B, Ohgi K, Zhang J, Rose DW, Fu X-D, Glass CK, et al. 2009. Nuclear receptor-induced chromosomal proximity and DNA breaks underlie specific translocations in cancer. *Cell* **139**: 1069–83. http://www.ncbi.nlm.nih.gov/pubmed/19962179.

Liu N, Lee CH, Swigut T, Grow E, Gu B, Bassik MC, Wysocka J. 2018. Selective silencing of euchromatic L1s revealed by genome-wide screens for L1 regulators. *Nature* **553**: 228–232. http://www.ncbi.nlm.nih.gov/pubmed/29211708.

Love MI, Huber W, Anders S. 2014. Moderated estimation of fold change and dispersion for RNA-seq data with DESeq2. *Genome Biol* **15**: 550. http://www.ncbi.nlm.nih.gov/pubmed/25516281.

Lukic S, Nicolas J-C, Levine AJ. 2014. The diversity of zinc-finger genes on human chromosome 19 provides an evolutionary mechanism for defense against inherited endogenous retroviruses. *Cell Death Differ* **21**: 381–7. http://www.ncbi.nlm.nih.gov/pubmed/24162661.

Lupo A, Cesaro E, Montano G, Zurlo D, Izzo P, Costanzo P. 2013. KRAB-Zinc Finger Proteins: A Repressor Family Displaying Multiple Biological Functions. *Curr Genomics* **14**: 268–78. http://www.ncbi.nlm.nih.gov/pubmed/24294107.

Lykoskoufis NMR, Planet E, Ongen H, Trono D, Dermitzakis ET. 2024. Transposable elements mediate genetic effects altering the expression of nearby genes in colorectal cancer. *Nat Commun* **15**: 749. http://www.ncbi.nlm.nih.gov/pubmed/38272908.

Macfarlan TS, Gifford WD, Driscoll S, Lettieri K, Rowe HM, Bonanomi D, Firth A, Singer O, Trono D, Pfaff SL. 2012. Embryonic stem cell potency fluctuates with endogenous retrovirus activity. *Nature* **487**: 57–63. http://www.ncbi.nlm.nih.gov/pubmed/22722858.

Maillet L, Tu C, Hong YK, Shuster EO, Collart MA. 2000. The essential function of Not1 lies within the Ccr4-Not complex. *J Mol Biol* **303**: 131–43. http://www.ncbi.nlm.nih.gov/pubmed/11023781.

Marzluff WF, Wagner EJ, Duronio RJ. 2008. Metabolism and regulation of canonical histone mRNAs: life without a poly(A) tail. *Nat Rev Genet* **9**: 843–54. http://www.ncbi.nlm.nih.gov/pubmed/18927579.

Mätlik K, Redik K, Speek M. 2006. L1 antisense promoter drives tissue-specific transcription of human genes. *J Biomed Biotechnol* **2006**: 71753. http://www.ncbi.nlm.nih.gov/pubmed/16877819.

Medina-Muñoz SG, Kushawah G, Castellano LA, Diez M, DeVore ML, Salazar MJB, Bazzini AA. 2021. Crosstalk between codon optimality and cis-regulatory elements dictates mRNA stability. *Genome Biol* **22**: 14. http://www.ncbi.nlm.nih.gov/pubmed/33402205.

Miller JE, Reese JC. 2012. Ccr4-Not complex: the control freak of eukaryotic cells. *Crit Rev Biochem Mol Biol* **47**: 315–33. http://www.ncbi.nlm.nih.gov/pubmed/22416820.

Morrissey A, Shi J, James DQ, Mahony S. 2024. Accurate allocation of multimapped reads enables regulatory element analysis at repeats. *Genome Res* **34**: 937–951. http://www.ncbi.nlm.nih.gov/pubmed/38986578.

Mostafa D, Takahashi A, Yanagiya A, Yamaguchi T, Abe T, Kureha T, Kuba K, Kanegae Y, Furuta Y, Yamamoto T, et al. 2020. Essential functions of the CNOT7/8 catalytic subunits of the CCR4-NOT complex in mRNA regulation and cell viability. *RNA Biol* **17**: 403–416. http://www.ncbi.nlm.nih.gov/pubmed/31924127.

Nadel J, Athanasiadou R, Lemetre C, Wijetunga NA, Ó Broin P, Sato H, Zhang Z, Jeddeloh J, Montagna C, Golden A, et al. 2015. RNA:DNA hybrids in the human genome have distinctive nucleotide characteristics, chromatin composition, and transcriptional relationships. *Epigenetics Chromatin* **8**: 46.

http://www.ncbi.nlm.nih.gov/pubmed/26579211.

Narula A, Ellis J, Taliaferro JM, Rissland OS. 2019. Coding regions affect mRNA stability in human cells. *RNA* **25**: 1751–1764. http://www.ncbi.nlm.nih.gov/pubmed/31527111.

Nielsen AL, Ortiz JA, You J, Oulad-Abdelghani M, Khechumian R, Gansmuller A, Chambon P, Losson R. 1999. Interaction with members of the heterochromatin protein 1 (HP1) family and histone deacetylation are differentially involved in transcriptional silencing by members of the TIF1 family. *EMBO J* **18**: 6385–95. http://www.ncbi.nlm.nih.gov/pubmed/10562550.

Osipovich AB, Dudek KD, Trinh LT, Kim LH, Shrestha S, Cartailler J-P, Magnuson MA. 2023. ZFP92, a KRAB domain zinc finger protein enriched in pancreatic islets, binds to B1/Alu SINE transposable elements and regulates retroelements and genes. *PLoS Genet* **19**: e1010729. http://www.ncbi.nlm.nih.gov/pubmed/37155670.

Panasenko OO, Collart MA. 2011. Not4 E3 ligase contributes to proteasome assembly and functional integrity in part through Ecm29. *Mol Cell Biol* **31**: 1610–23. http://www.ncbi.nlm.nih.gov/pubmed/21321079.

Pavanello L, Hall B, Airhihen B, Winkler GS. 2018. The central region of CNOT1 and CNOT9 stimulates deadenylation by the Ccr4-Not nuclease module. *Biochem J* **475**: 3437–3450. http://www.ncbi.nlm.nih.gov/pubmed/30309886.

Pavanello L, Hall M, Winkler GS. 2023. Regulation of eukaryotic mRNA deadenylation and degradation by the Ccr4-Not complex. *Front cell Dev Biol* **11**: 1153624. http://www.ncbi.nlm.nih.gov/pubmed/37152278.

Petit A-P, Wohlbold L, Bawankar P, Huntzinger E, Schmidt S, Izaurralde E, Weichenrieder O. 2012. The structural basis for the interaction between the CAF1 nuclease and the NOT1 scaffold of the human CCR4-NOT deadenylase complex. *Nucleic Acids Res* **40**: 11058–72. http://www.ncbi.nlm.nih.gov/pubmed/22977175.

Pfannenstein J, Tyryshkin M, Gulden ME, Doud EH, Mosley AL, Reese JC. 2024. Characterization of BioID tagging systems in budding yeast and exploring the interactome of the Ccr4-Not complex. *bioRxiv Prepr Serv Biol*. http://www.ncbi.nlm.nih.gov/pubmed/38766143.

Poetz F, Corbo J, Levdansky Y, Spiegelhalter A, Lindner D, Magg V, Lebedeva S, Schweiggert J, Schott J, Valkov E, et al. 2021. RNF219 attenuates global mRNA decay through inhibition of CCR4-NOT complex-mediated deadenylation. *Nat Commun* **12**: 7175. http://www.ncbi.nlm.nih.gov/pubmed/34887419.

Pontis J, Pulver C, Playfoot CJ, Planet E, Grun D, Offner S, Duc J, Manfrin A, Lutolf MP, Trono D. 2022. Primate-specific transposable elements shape transcriptional networks during human development. *Nat Commun*

13: 7178. http://www.ncbi.nlm.nih.gov/pubmed/36418324.

Presnyak V, Alhusaini N, Chen Y-H, Martin S, Morris N, Kline N, Olson S, Weinberg D, Baker KE, Graveley BR, et al. 2015. Codon optimality is a major determinant of mRNA stability. *Cell* **160**: 1111–24. http://www.ncbi.nlm.nih.gov/pubmed/25768907.

Reese JC. 2013. The control of elongation by the yeast Ccr4-not complex. *Biochim Biophys Acta* **1829**: 127–33. http://www.ncbi.nlm.nih.gov/pubmed/22975735.

Rosspopoff O, Trono D. 2023. Take a walk on the KRAB side. *Trends Genet* **39**: 844–857. http://www.ncbi.nlm.nih.gov/pubmed/37716846.

Ryan RF, Schultz DC, Ayyanathan K, Singh PB, Friedman JR, Fredericks WJ, Rauscher FJ. 1999. KAP-1 corepressor protein interacts and colocalizes with heterochromatic and euchromatic HP1 proteins: a potential role for Krüppel-associated box-zinc finger proteins in heterochromatin-mediated gene silencing. *Mol Cell Biol* **19**: 4366–78. http://www.ncbi.nlm.nih.gov/pubmed/10330177.

Schultz DC, Ayyanathan K, Negorev D, Maul GG, Rauscher FJ. 2002. SETDB1: a novel KAP-1-associated histone H3, lysine 9-specific methyltransferase that contributes to HP1-mediated silencing of euchromatic genes by KRAB zinc-finger proteins. *Genes Dev* **16**: 919–32. http://www.ncbi.nlm.nih.gov/pubmed/11959841.

Schultz DC, Friedman JR, Rauscher FJ. 2001. Targeting histone deacetylase complexes via KRAB-zinc finger proteins: the PHD and bromodomains of KAP-1 form a cooperative unit that recruits a novel isoform of the Mi-2alpha subunit of NuRD. *Genes Dev* **15**: 428–43. http://www.ncbi.nlm.nih.gov/pubmed/11230151.

Schwalb B, Michel M, Zacher B, Frühauf K, Demel C, Tresch A, Gagneur J, Cramer P. 2016. TT-seq maps the human transient transcriptome. *Science* **352**: 1225–8. http://www.ncbi.nlm.nih.gov/pubmed/27257258.

Sears RM, May DG, Roux KJ. 2019. BioID as a Tool for Protein-Proximity Labeling in Living Cells. *Methods Mol Biol* **2012**: 299–313. http://www.ncbi.nlm.nih.gov/pubmed/31161514.

Shalem O, Dahan O, Levo M, Martinez MR, Furman I, Segal E, Pilpel Y. 2008. Transient transcriptional responses to stress are generated by opposing effects of mRNA production and degradation. *Mol Syst Biol* **4**: 223. http://www.ncbi.nlm.nih.gov/pubmed/18854817.

Shalem O, Groisman B, Choder M, Dahan O, Pilpel Y. 2011. Transcriptome kinetics is governed by a genome-wide coupling of mRNA production and degradation: a role for RNA Pol II. *PLoS Genet* **7**: e1002273. http://www.ncbi.nlm.nih.gov/pubmed/21931566.

Shannon M, Ashworth LK, Mucenski ML, Lamerdin JE, Branscomb E, Stubbs L. 1996. Comparative analysis of a conserved zinc finger gene cluster on human chromosome 19q and mouse chromosome 7. *Genomics* **33**: 112–20. http://www.ncbi.nlm.nih.gov/pubmed/8617494.

Shirai Y-T, Suzuki T, Morita M, Takahashi A, Yamamoto T. 2014. Multifunctional roles of the mammalian CCR4-NOT complex in physiological phenomena. *Front Genet* **5**: 286. http://www.ncbi.nlm.nih.gov/pubmed/25191340.

Speek M. 2001. Antisense promoter of human L1 retrotransposon drives transcription of adjacent cellular genes. *Mol Cell Biol* **21**: 1973–85. http://www.ncbi.nlm.nih.gov/pubmed/11238933.

Tani H, Mizutani R, Salam KA, Tano K, Ijiri K, Wakamatsu A, Isogai T, Suzuki Y, Akimitsu N. 2012. Genome-wide determination of RNA stability reveals hundreds of short-lived noncoding transcripts in mammals. *Genome Res* **22**: 947–56. http://www.ncbi.nlm.nih.gov/pubmed/22369889.

Temme C, Zhang L, Kremmer E, Ihling C, Chartier A, Sinz A, Simonelig M, Wahle E. 2010. Subunits of the Drosophila CCR4-NOT complex and their roles in mRNA deadenylation. *RNA* **16**: 1356–70. http://www.ncbi.nlm.nih.gov/pubmed/20504953.

Timmers HTM, Tora L. 2018. Transcript Buffering: A Balancing Act between mRNA Synthesis and mRNA Degradation. *Mol Cell* **72**: 10–17. http://www.ncbi.nlm.nih.gov/pubmed/30290147.

Titov D V, Gilman B, He Q-L, Bhat S, Low W-K, Dang Y, Smeaton M, Demain AL, Miller PS, Kugel JF, et al. 2011. XPB, a subunit of TFIIH, is a target of the natural product triptolide. *Nat Chem Biol* **7**: 182–8. http://www.ncbi.nlm.nih.gov/pubmed/21278739.

Traven A, Hammet A, Tenis N, Denis CL, Heierhorst J. 2005. Ccr4-not complex mRNA deadenylase activity contributes to DNA damage responses in Saccharomyces cerevisiae. *Genetics* **169**: 65–75. http://www.ncbi.nlm.nih.gov/pubmed/15466434.

Vieux K-F, Clarke HJ. 2018. CNOT6 regulates a novel pattern of mRNA deadenylation during oocyte meiotic maturation. *Sci Rep* **8**: 6812. http://www.ncbi.nlm.nih.gov/pubmed/29717177.

Vogel MJ, Guelen L, de Wit E, Peric-Hupkes D, Lodén M, Talhout W, Feenstra M, Abbas B, Classen A-K, van Steensel B. 2006. Human heterochromatin proteins form large domains containing KRAB-ZNF genes. *Genome Res* **16**: 1493–504. http://www.ncbi.nlm.nih.gov/pubmed/17038565.

Wang Y, Lu J, He L, Yu Q. 2011. Triptolide (TPL) inhibits global transcription by inducing proteasome-dependent

degradation of RNA polymerase II (Pol II). *PLoS One* **6**: e23993. http://www.ncbi.nlm.nih.gov/pubmed/21931633.

Wolf G, de Iaco A, Sun M-A, Bruno M, Tinkham M, Hoang D, Mitra A, Ralls S, Trono D, Macfarlan TS. 2020. KRAB-zinc finger protein gene expansion in response to active retrotransposons in the murine lineage. *Elife* **9**. http://www.ncbi.nlm.nih.gov/pubmed/32479262.

Wu Q, Medina SG, Kushawah G, DeVore ML, Castellano LA, Hand JM, Wright M, Bazzini AA. 2019. Translation affects mRNA stability in a codon-dependent manner in human cells. *Elife* **8**. http://www.ncbi.nlm.nih.gov/pubmed/31012849.

Youn J-Y, Dunham WH, Hong SJ, Knight JDR, Bashkurov M, Chen GI, Bagci H, Rathod B, MacLeod G, Eng SWM, et al. 2018. High-Density Proximity Mapping Reveals the Subcellular Organization of mRNA-Associated Granules and Bodies. *Mol Cell* **69**: 517-532.e11. http://www.ncbi.nlm.nih.gov/pubmed/29395067.

Zhang Q, Pavanello L, Potapov A, Bartlam M, Winkler GS. 2022. Structure of the human Ccr4-Not nuclease module using X-ray crystallography and electron paramagnetic resonance spectroscopy distance measurements. *Protein Sci* **31**: 758–764. http://www.ncbi.nlm.nih.gov/pubmed/34923703.

Figure legends

Figure 1. Auxin inducible degron system to deplete CNOT1 and CNOT4. (A, B) Western blot analysis of parental (DLD-1^{TIR1+}), CNOT1^{AID} and CNOT4^{AID} cells. Two different amounts of lysates (differing by a factor of 2) were loaded onto SDS-PAGE followed immunoblot analysis using antibodies against CNOT1 in (**A)** or CNOT4 in **B).** Ddx6 was used as a loading control. CNOT1^{AID} or CNOT4^{AID} cells were treated with ± 1mM auxin containing media for 2, 4, 8 and 24 h (C and D). Multiple bands detected in CNOT1 blots may represent degradation products or versions with posttranslational modifications. The bands in CNOT4 blots may represent alternate splice isoforms and/or isoforms with alternate translation start sites. The asterisk (in **B** and **D**) represents a non-specific band detected by anti CNOT4 antibody.

Figure 2. Depletion of CNOT1, but not CNOT4 leads to the destruction of the CCR4-NOT complex. Benzonase-treated extracts from CNOT1^{AID} (**A**) or CNOT4^{AID} (**B**) cells cultured in ± 1mM were subjected to size exclusion chromatography. The fractions were concentrated by TCA precipitation and subjected to immunoblotting for hCCR4-NOT subunits. The red arrow on CNOT6 blot indicates the specific band. Fractions containing the CCR4-NOT complex are shown. Molecular weights of calibration proteins are shown on top. For each blot against a particular subunit, multiple images were spliced together. Vertical lines represent those splicing junctions. (Vo = the void volume).

Figure 3. Identification of CNOT1 and CNOT4 interacting proteins by proximity labelling (BioID). (A, B) Volcano-plots of log_2Fold-enrichment (FE) in relative protein intensity of biotinylated proteins versus negative log_{10} of p-values. Datapoints in red identify proteins meeting a ≥ 1.5 enrichment and p-adj < 0.05 cutoff. CCR4-NOT complex subunits are marked with a black circle with CNOT1 and CNOT4 indicated by arrows. **(A)** Comparison of proteins from CNOT1^{mTID} versus control cells. **(B)** Data for the comparison between CNOT4^{TID} versus control cells. **(C)** Gene Ontology terms of 'cellular component' of enriched proteins meeting the cutoff values in **A** (CNOT1^{mTID}/control). Proteins dataset was analyzed using ShinyGO 0.80 and GO categories with an enrichment FDR < 0.01 are shown. **(D)** Same as in **C**, except the CNOT4-enriched interacting proteins (CNOT4^{TID}/control). **(E)** Venn diagram showing the overlap of CNOT1 and CNOT4 enriched proteins. The p-value for the overlap was calculated using RStudio.

Figure 4. Effects of CNOT1 and CNOT4 depletion of steady-state RNA levels. (A, B, C) Volcano-plots of log_2FoldChange (FC) in steady-state RNA levels versus negative log_{10} of p-values. CNOT1 or CNOT4 were depleted with media containing 1mM auxin for 2 h (**A**), 8 h (**B**) and 24 h (**C**). The numbers in each panel represent differentially expressed genes with a FC ≥ 1.5 and p-adj < 0.01. For 2 h datapoint FCs were calculated by comparing

RNA levels between auxin treated CNOT1^{AID} cells or CNOT4^{AID} cells (depleted) v/s auxin treated parental cells (non-depleted). For **A, B and C**, each dot represents an individual RNA.

Figure 5. Depletion of CNOT1 and CNOT4 have opposite transcriptome-wide effects on RNA half-lives. (A) Schematic depicting the experimental design to determine RNA half-lives. **(B)** Scatter plot of RNA half-lives calculated in control (parental cells +auxin) and CNOT1 depleted cells (CNOT1^{AID} +auxin). **(C)** Scatter plot of RNA half-lives calculated in control (parental cells +auxin) and CNOT4 depleted cells (CNOT4^{AID} +auxin). **(D)** Boxplot analysis of RNA half-lives. p-values were calculated using the Mann Whitney Test between CNOT1 and CNOT4 depleted cells versus control cells. Total number of datapoints (N) and median half-life (M, in h) are shown **(E)** Cumulative fraction distribution plots of RNA half-lives in control and CNOT1 and CNOT4 depletion conditions. Kolmogorov-Smirnov (KS) statistic is shown. **(F)** Boxplot analysis of change in RNA half-lives upon CNOT1 and CNOT4 depletion for all and non-polyadenylated histone mRNAs. 'All' correspond to all RNAs whose foldchange in RNA half-life could be calculated under the experimental conditions (N = 16240, for CNOT1 dep/Control; N = 17238 for CNOT4 dep/Control). Sixty-one non-polyadenylated histone mRNAs were included in the analysis and polyadenylated histones were excluded.

Figure 6. Effects of CNOT1 and CNOT4 depletion on mRNA half-lives are a function of the codon optimality. (A) Scatterplot of transcript average codon stability coefficients (Avg. CSC) calculated from (Forrest et al. 2020) versus RNA half-lives measured in this study (N = 1054). Only mRNAs represented in both studies were used. **(B)** Transcripts were grouped into less optimal (Avg. CSC < 0, highlighted in red) and more optimal (Avg. CSC > 0, highlighted in blue) and cumulative fraction distribution plots for RNA half-lives measured in this study were plotted. Total number of data points in each group (N), median half-life (M, in h) and Kolmogorov-Smirnov statistic are shown. **(C)** Scatterplots of Avg. CSC versus fold-change in RNA half-life upon CNOT1 depletion (orange datapoints) or CNOT4 depletion (purple datapoints). **(D)** Cumulative fraction distribution plot of fold-changes in RNA half-lives versus CSC. Groups of transcripts analyzed here are defined above in **B**. M corresponds to median fold-change in RNA half-life upon CNOT1 depletion as compared to control. **(E)** Same as in **D**, except the data from CNOT4 depleted cells. For **A** and **C** - Total number of datapoints (N), Spearman Rank Correlation rho (rho) and 2-sided p-value of significance for correlation are shown.

Figure 7. Depletion of CNOT1 or CNOT4 leads to rapid decrease in nascent transcription of KRAB Zinc Finger genes on chromosome 19. (A) K-means clustering of fold-changes (FCs) in RNA transcription of all genes calculated by TT-seq. The rows of the heatmap represent individual RNAs (N = 23961). FC data were used to make heatmaps in 'Cluster 3.0' (K = 3 and 'Euclidean distance' as a similarity metric) and were visualized by 'Java TreeView'. **(B)** Distribution of genes in the top enriched GO category in figure **S12B** (N = 143). ZNFs were grouped as with or

without KRAB domain, based on (de Tribolet-Hardy et al. 2023). **(C)** K-means clustering of FC in transcription of ZNF genes determined by TT-seq (N= 642). Heatmap was generated as described in **A**. **(D)** Venn diagram showing overlap of DTGs (blue and red dots in Figure S11E-F) and genes showing at least one KZFP binding peak. Data from repressed KZFPs with highest number of genome-wide peaks were analyzed. **(E)** Analysis of fraction of KZFP peaks in genes which are transcriptionally either 'Up' or 'Down' in CNOT1/4 depletion conditions.

Figure 8. Depletion of CNOT1 or CNOT4 leads to activation of LINEs and other repeat elements. (A) Boxplot analysis of changes in transcription of KRAB-ZNFs (KZNFs) genes after 8 h depletion of CNOT1 or CNOT4. KZNFs were binned based on their location on chromosome 19 or other chromosomes based on (de Tribolet-Hardy et al. 2023). Total number of datapoints (N), median fold-change (M) and P-values by Mann Whitney Test (compared to All) are indicated in the panel. **(B, C)** Distribution of repeat elements whose transcription was differentially regulated (FC > 1.5 and p-adj < 0.05) in CNOT1- (**B**) and CNOT4-depleted cells (**C**). The fold-change in expression was determined by DESEq2 analysis of RNA expression measured by TT-seq as described in Figure **S11B**. **(D, E)** K-means clustering of fold-changes in transcription of LINEs upon depletion of CNOT1 or CNOT4 for 2 h (**D**) or 8 h (**E**). **(F, G)** Correlation plots between fold-change in transcription (TT-seq) of LINE elements versus that of its nearest gene upon 8 h depletion of CNOT1 (**F**) or CNOT4 (**G**). Top10 KZFPs with highest number of genome-wide peaks based on (Imbeault et al. 2017) and whose transcription was repressed upon CNOT1 or4 depletion were analyzed (as in Figure 7D-E). LINEs associated with these KZFPs were mapped and the nearest gene was located for each LINE followed by correlation analysis. Number of datapoints (N), Spearman correlation (rho) and 2-sided p-value are shown on each plot.

Figure 1

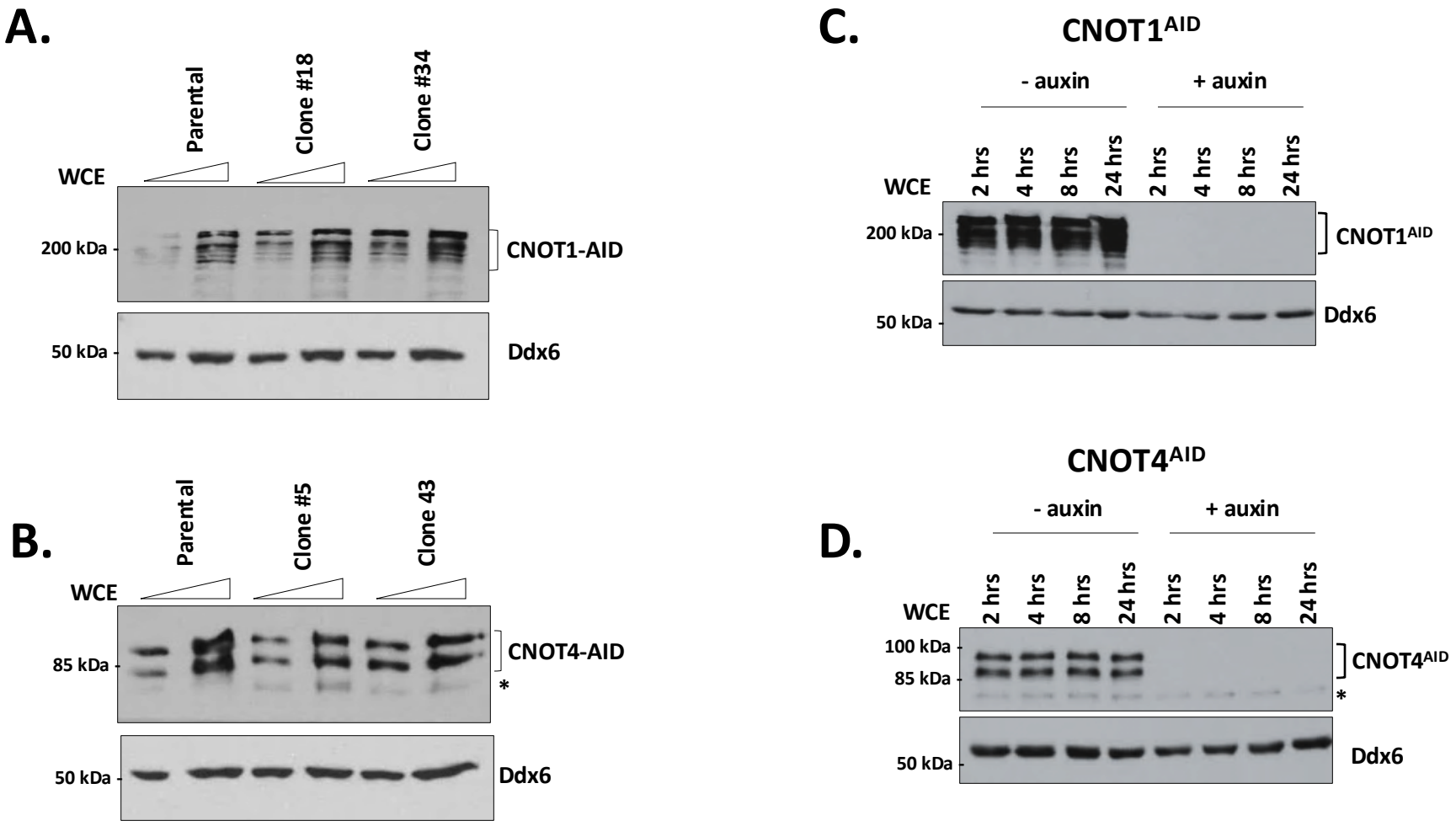
A.
Parental
Clone #18
Clone #34
WCE
200 kDa
CNOT1-AID
50 kDa
Ddx6
B.
Parental
Clone #5
Clone 43
WCE
85 kDa
CNOT4-AID
*
50 kDa
Ddx6
C.
CNOT1AID
- auxin
+ auxin
2 hrs
4 hrs
8 hrs
24 hrs
2 hrs
4 hrs
8 hrs
24 hrs
WCE
200 kDa
CNOT1AID
50 kDa
Ddx6
D.
CNOT4AID
- auxin
+ auxin
2 hrs
4 hrs
8 hrs
24 hrs
2 hrs
4 hrs
8 hrs
24 hrs
WCE
100 kDa
85 kDa
CNOT4AID
*
50 kDa
Ddx6

Figure 2

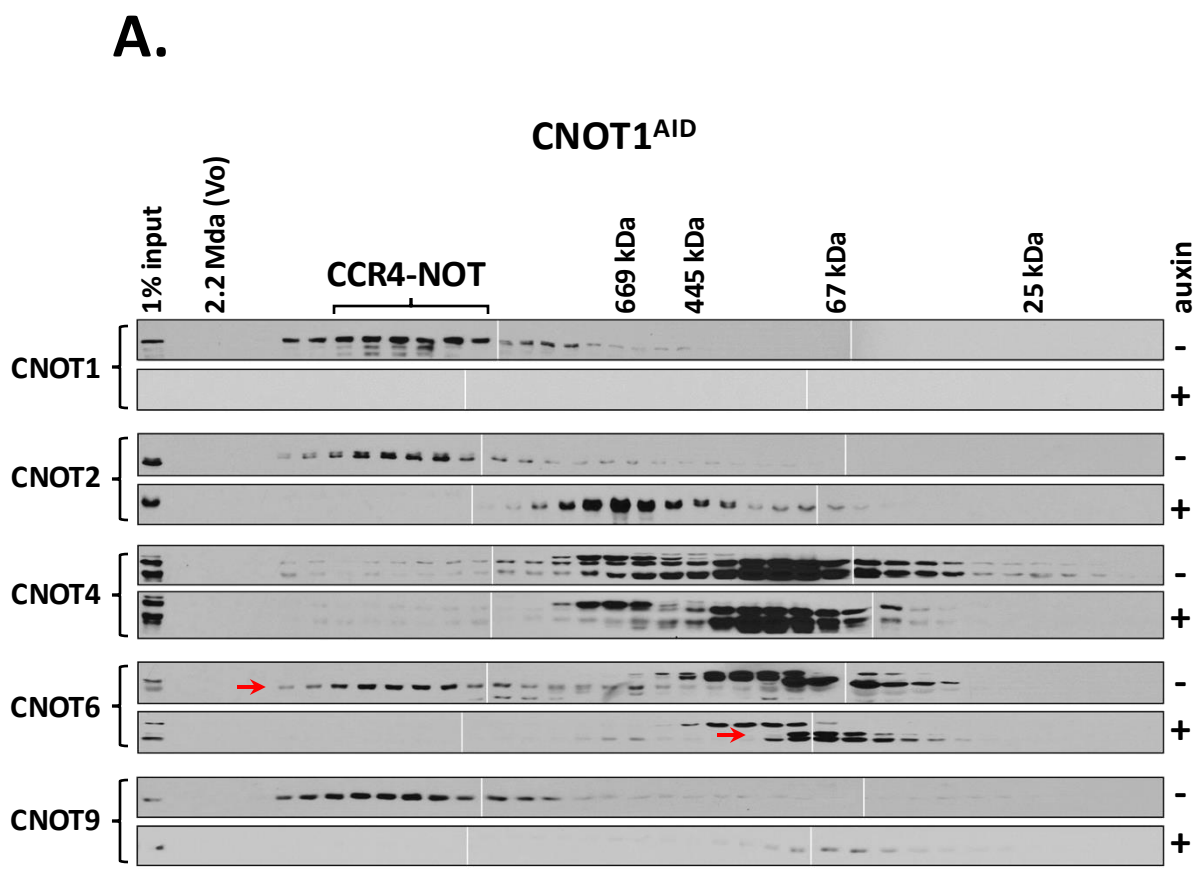
A.
CNOT1AID
1% input
2.2 Mda (Vo)
CCR4-NOT
669 kDa
445 kDa
67 kDa
25 kDa
auxin
CNOT1
CNOT2
CNOT4
CNOT6
CNOT9
-
+

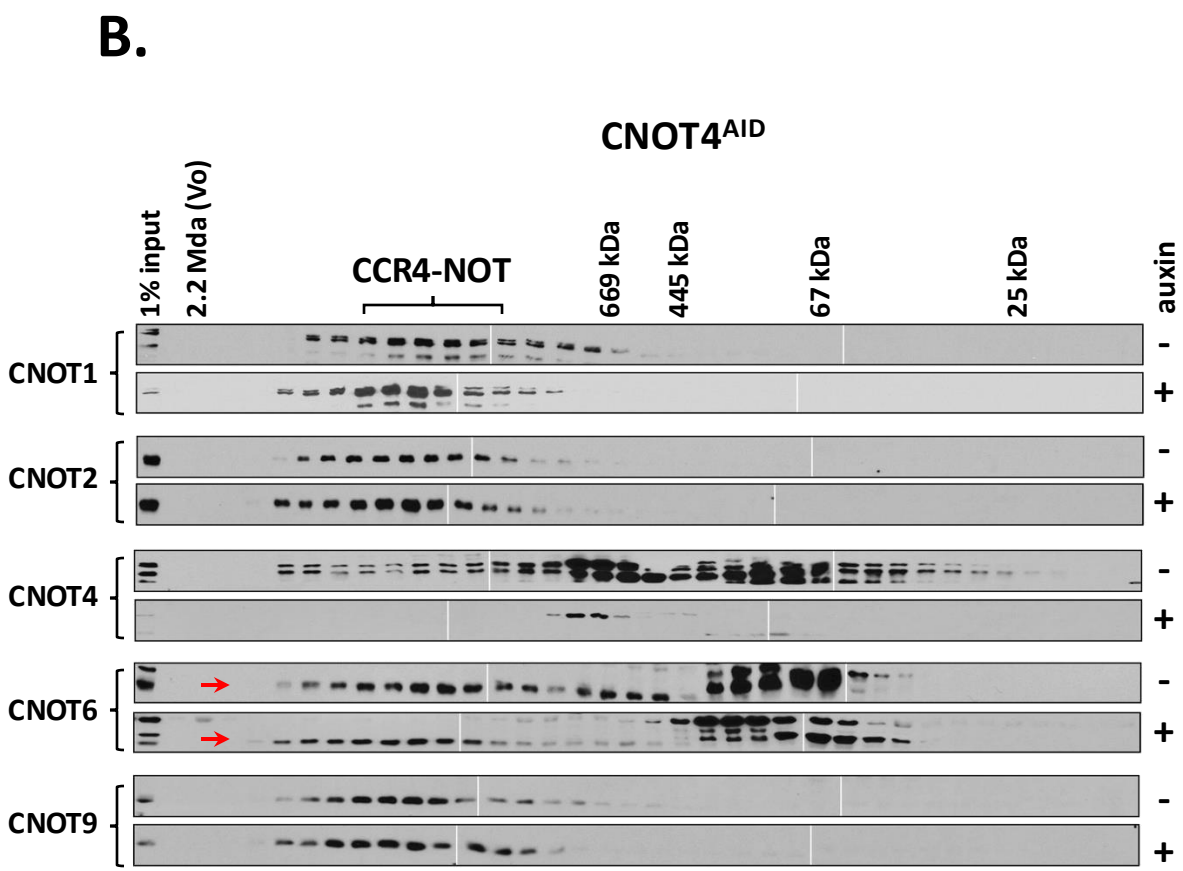
B.
CNOT4AID
1% input
2.2 Mda (Vo)
CCR4-NOT
669 kDa
445 kDa
67 kDa
25 kDa
auxin
CNOT1
CNOT2
CNOT4
CNOT6
CNOT9
-
+

Figure 3

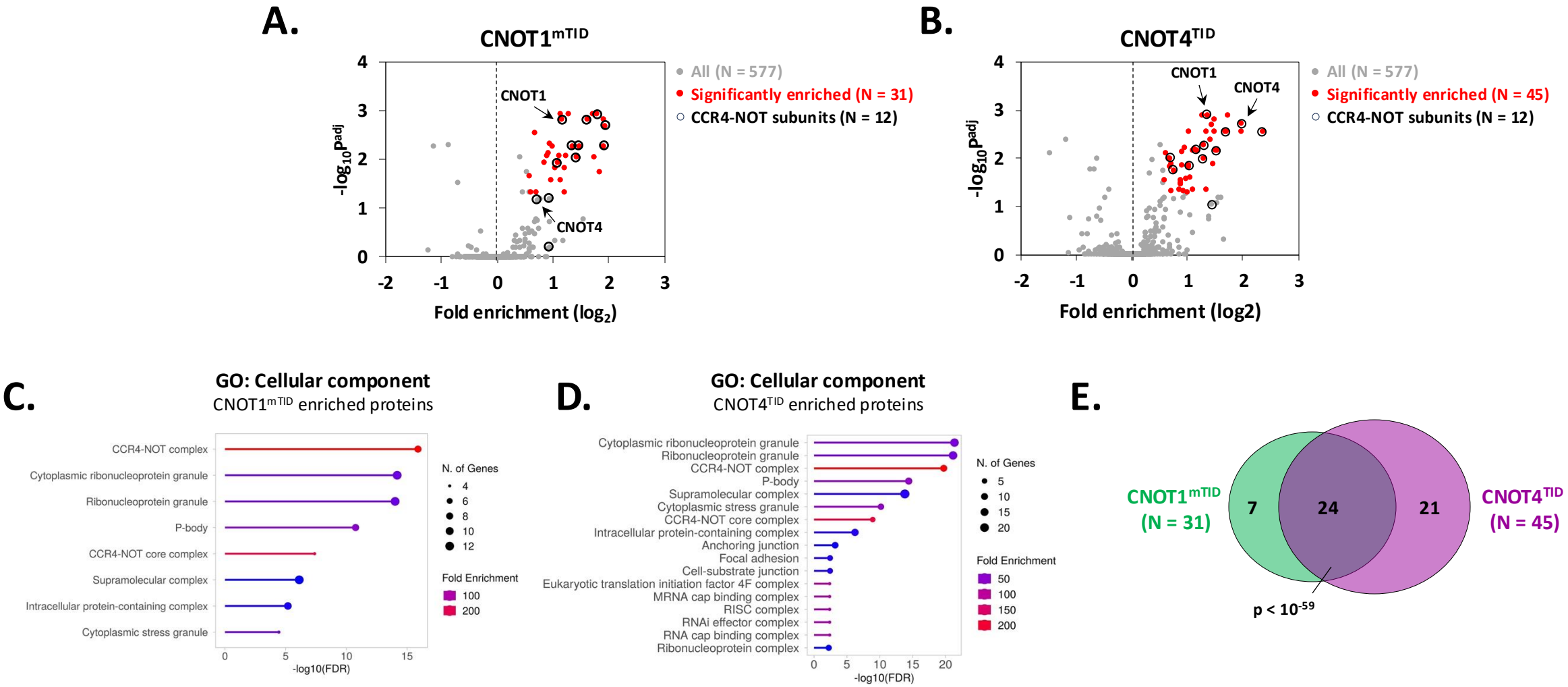
A.
CNOT1mTID
CNOT1
CNOT4
-log10Padj
Fold enrichment (log2)
All (N = 577)
Significantly enriched (N = 31)
CCR4-NOT subunits (N = 12)
B.
CNOT4TID
CNOT1
CNOT4
-log10Padj
Fold enrichment (log2)
All (N = 577)
Significantly enriched (N = 45)
CCR4-NOT subunits (N = 12)
C.
GO: Cellular component
CNOT1mTID enriched proteins
CCR4-NOT complex
Cytoplasmic ribonucleoprotein granule
Ribonucleoprotein granule
P-body
CCR4-NOT core complex
Supramolecular complex
Intracellular protein-containing complex
Cytoplasmic stress granule
-log10(FDR)
N. of Genes
Fold Enrichment
D.
GO: Cellular component
CNOT4TID enriched proteins
Cytoplasmic ribonucleoprotein granule
Ribonucleoprotein granule
CCR4-NOT complex
P-body
Supramolecular complex
Cytoplasmic stress granule
CCR4-NOT core complex
Intracellular protein-containing complex
Anchoring junction
Focal adhesion
Cell-substrate junction
Eukaryotic translation initiation factor 4F complex
MRNA cap binding complex
RISC complex
RNAi effector complex
RNA cap binding complex
Ribonucleoprotein complex
-log10(FDR)
N. of Genes
Fold Enrichment
E.
CNOT1mTID
(N = 31)
7
24
21
CNOT4TID
(N = 45)
p < 10-59

Figure 4

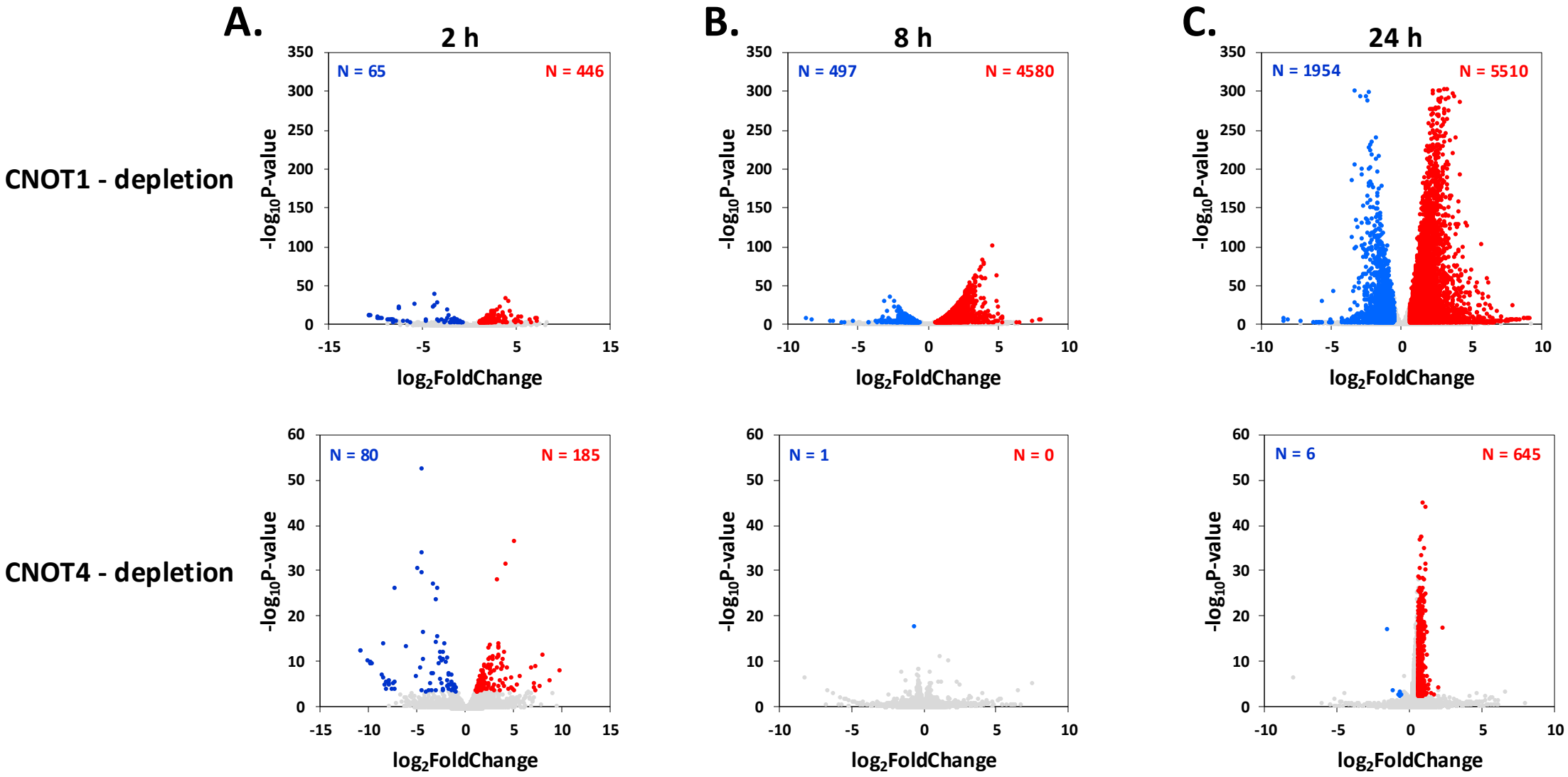
A.
2 h
B.
8 h
C.
24 h
CNOT1 - depletion
CNOT4 - depletion
N = 65
N = 446
N = 497
N = 4580
N = 1954
N = 5510
N = 80
N = 185
N = 1
N = 0
N = 6
N = 645
-log10P-value
log2FoldChange

Figure 5

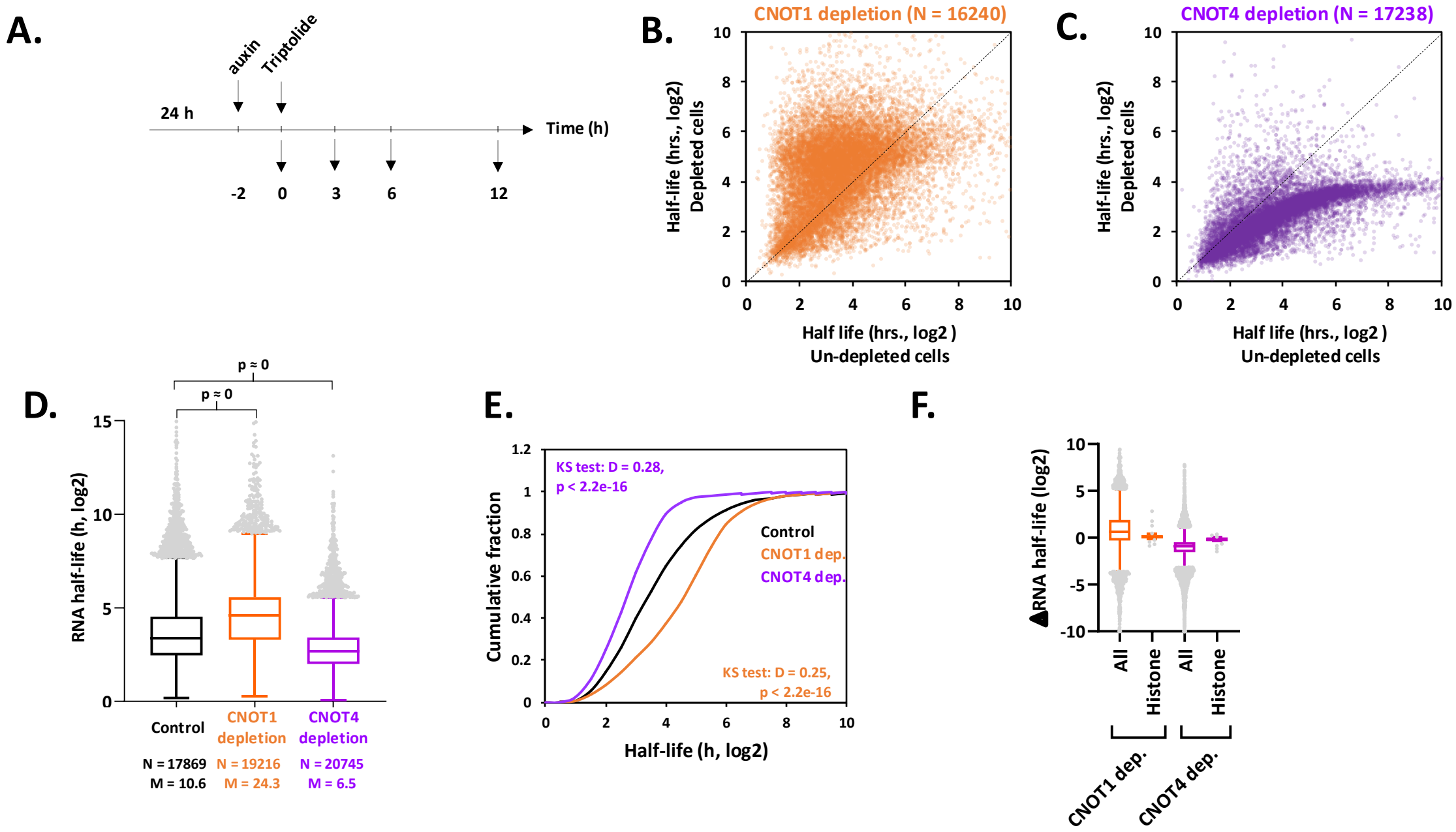
A.
auxin
Triptolide
24 h
Time (h)
-2
0
3
6
12
B.
CNOT1 depletion (N = 16240)
Half-life (hrs., log2) Depleted cells
Half life (hrs., log2) Un-depleted cells
C.
CNOT4 depletion (N = 17238)
Half-life (hrs., log2) Depleted cells
Half life (hrs., log2) Un-depleted cells
D.
p ≈ 0
p ≈ 0
RNA half-life (h, log2)
Control
CNOT1 depletion
CNOT4 depletion
N = 17869
M = 10.6
N = 19216
M = 24.3
N = 20745
M = 6.5
E.
KS test: D = 0.28, p < 2.2e-16
Control
CNOT1 dep.
CNOT4 dep.
KS test: D = 0.25, p < 2.2e-16
Cumulative fraction
Half-life (h, log2)
F.
ΔRNA half-life (log2)
All
Histone
All
Histone
CNOT1 dep.
CNOT4 dep.

Figure 6

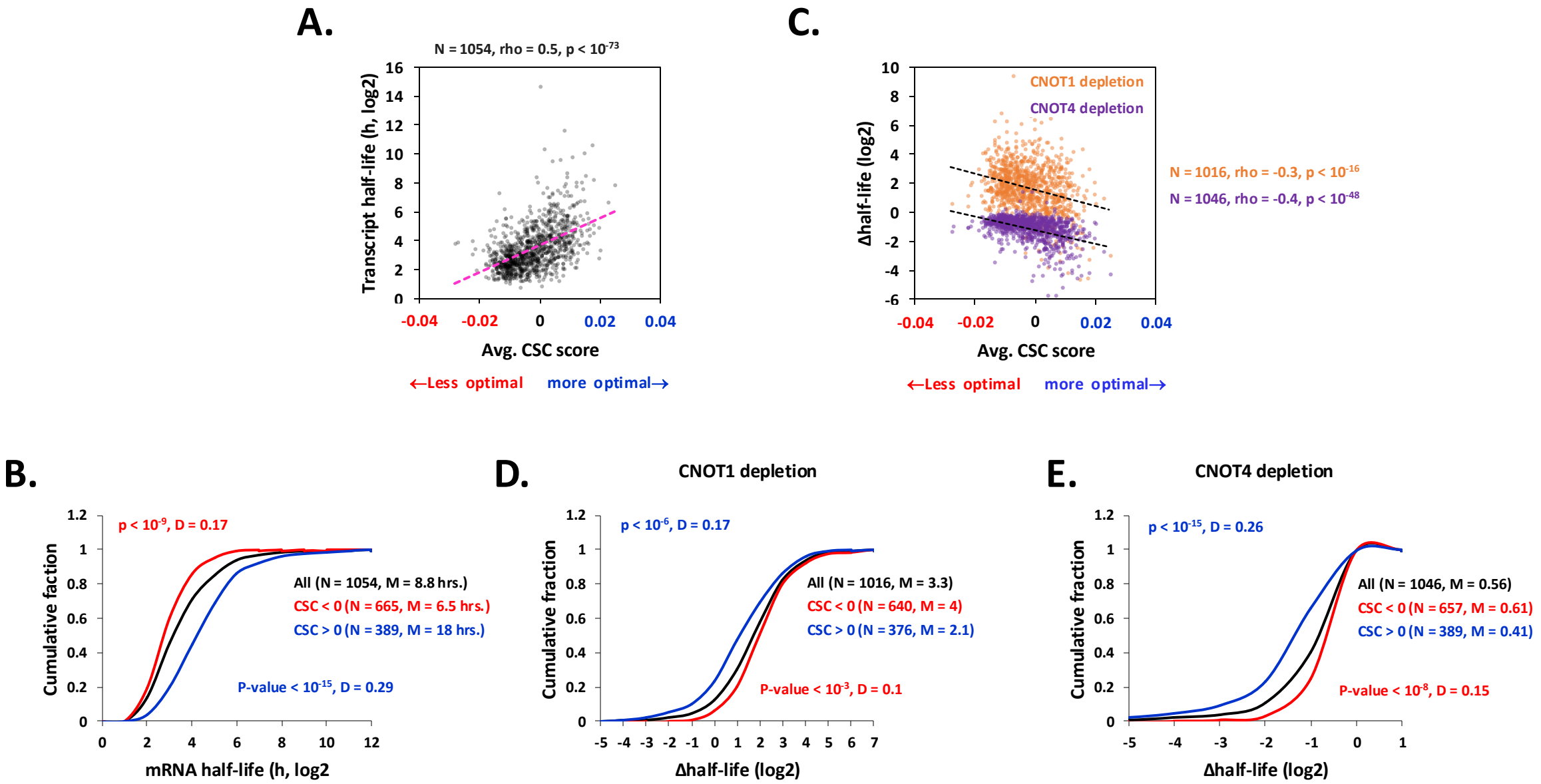
A.
N = 1054, rho = 0.5, p < 10-73
Transcript half-life (h, log2)
Avg. CSC score
←Less optimal
more optimal→
C.
CNOT1 depletion
CNOT4 depletion
N = 1016, rho = -0.3, p < 10-16
N = 1046, rho = -0.4, p < 10-48
Δhalf-life (log2)
Avg. CSC score
←Less optimal
more optimal→
B.
p < 10-9, D = 0.17
All (N = 1054, M = 8.8 hrs.)
CSC < 0 (N = 665, M = 6.5 hrs.)
CSC > 0 (N = 389, M = 18 hrs.)
P-value < 10-15, D = 0.29
Cumulative faction
mRNA half-life (h, log2
D.
CNOT1 depletion
p < 10-6, D = 0.17
All (N = 1016, M = 3.3)
CSC < 0 (N = 640, M = 4)
CSC > 0 (N = 376, M = 2.1)
P-value < 10-3, D = 0.1
Cumulative fraction
Δhalf-life (log2)
E.
CNOT4 depletion
p < 10-15, D = 0.26
All (N = 1046, M = 0.56)
CSC < 0 (N = 657, M = 0.61)
CSC > 0 (N = 389, M = 0.41)
P-value < 10-8, D = 0.15
Cumulative fraction
Δhalf-life (log2)

Figure 7

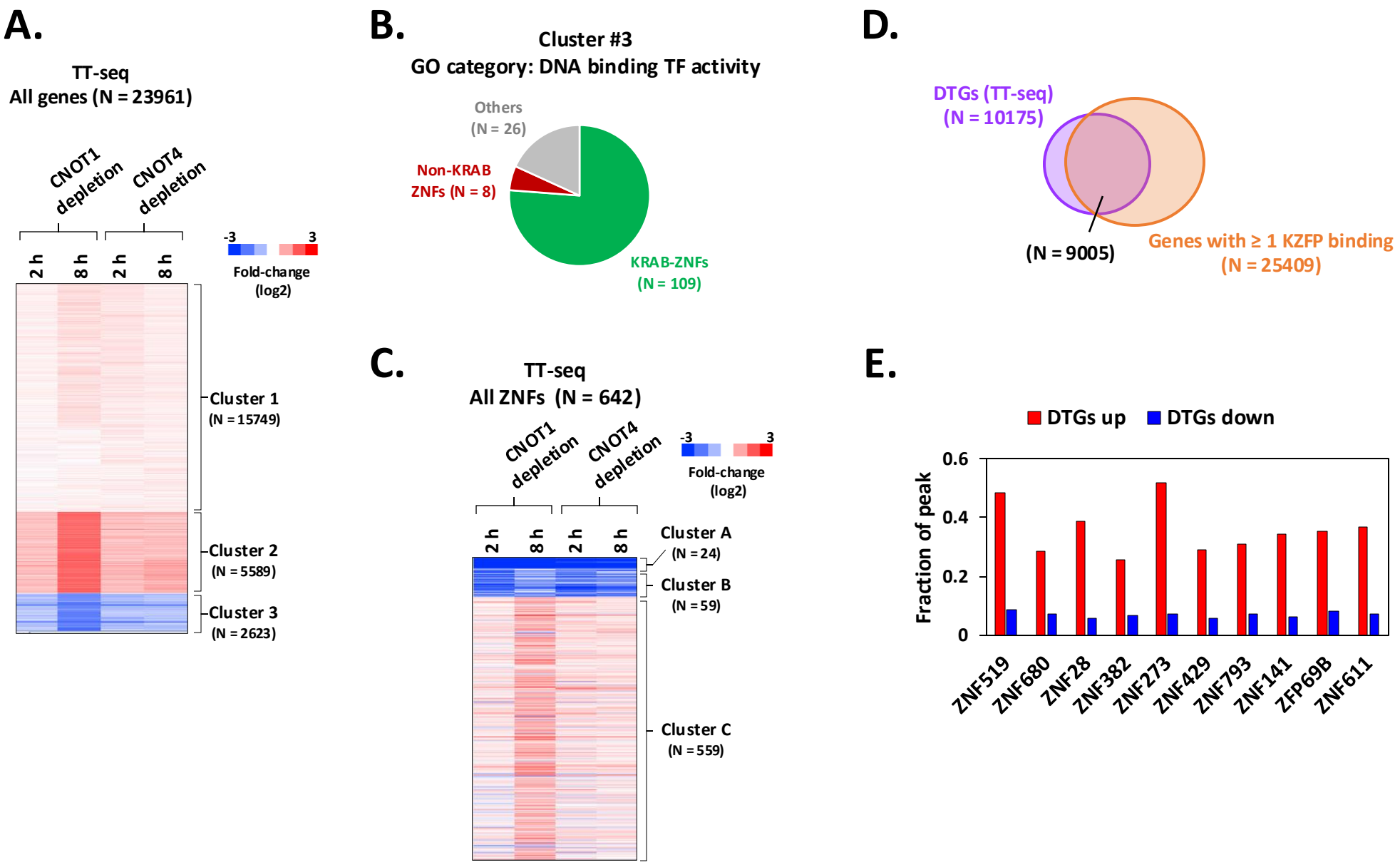
A.
TT-seq
All genes (N = 23961)
CNOT1 depletion
CNOT4 depletion
2 h
8 h
2 h
8 h
-3
3
Fold-change (log2)
Cluster 1 (N = 15749)
Cluster 2 (N = 5589)
Cluster 3 (N = 2623)
B.
Cluster #3
GO category: DNA binding TF activity
Others (N = 26)
Non-KRAB ZNFs (N = 8)
KRAB-ZNFs (N = 109)
C.
TT-seq
All ZNFs (N = 642)
CNOT1 depletion
CNOT4 depletion
2 h
8 h
2 h
8 h
-3
3
Fold-change (log2)
Cluster A (N = 24)
Cluster B (N = 59)
Cluster C (N = 559)
D.
DTGs (TT-seq) (N = 10175)
(N = 9005)
Genes with ≥ 1 KZFP binding (N = 25409)
E.
DTGs up
DTGs down
Fraction of peak
0.6
0.4
0.2
0
ZNF519
ZNF680
ZNF28
ZNF382
ZNF273
ZNF429
ZNF793
ZNF141
ZFP69B
ZNF611

Figure 8

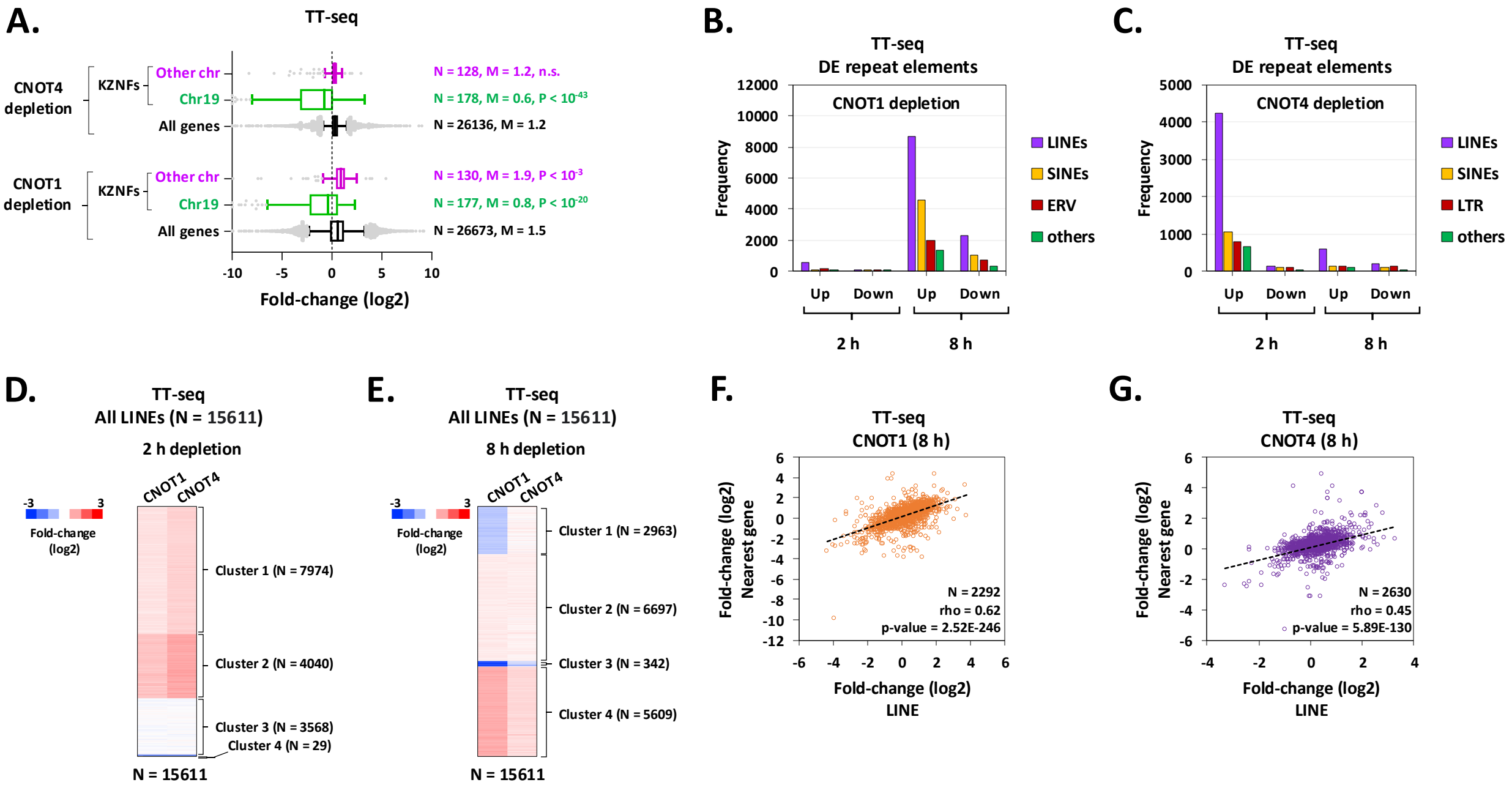
A.
TT-seq
CNOT4 depletion
KZNFs
Other chr
Chr19
All genes
N = 128, M = 1.2, n.s.
N = 178, M = 0.6, P < 10-43
N = 26136, M = 1.2
CNOT1 depletion
KZNFs
Other chr
Chr19
All genes
N = 130, M = 1.9, P < 10-3
N = 177, M = 0.8, P < 10-20
N = 26673, M = 1.5
-10 -5 0 5 10
Fold-change (log2)
B.
TT-seq
DE repeat elements
CNOT1 depletion
Frequency
12000 10000 8000 6000 4000 2000 0
Up Down Up Down
2 h 8 h
LINEs
SINEs
ERV
others
C.
TT-seq
DE repeat elements
CNOT4 depletion
Frequency
5000 4000 3000 2000 1000 0
Up Down Up Down
2 h 8 h
LINEs
SINEs
LTR
others
D.
TT-seq
All LINEs (N = 15611)
2 h depletion
-3 3
Fold-change (log2)
CNOT1 CNOT4
Cluster 1 (N = 7974)
Cluster 2 (N = 4040)
Cluster 3 (N = 3568)
Cluster 4 (N = 29)
N = 15611
E.
TT-seq
All LINEs (N = 15611)
8 h depletion
-3 3
Fold-change (log2)
CNOT1 CNOT4
Cluster 1 (N = 2963)
Cluster 2 (N = 6697)
Cluster 3 (N = 342)
Cluster 4 (N = 5609)
N = 15611
F.
TT-seq
CNOT1 (8 h)
Fold-change (log2) Nearest gene
6 4 2 0 -2 -4 -6 -8 -10 -12
N = 2292
rho = 0.62
p-value = 2.52E-246
-6 -4 -2 0 2 4 6
Fold-change (log2) LINE
G.
TT-seq
CNOT4 (8 h)
Fold-change (log2) Nearest gene
6 4 2 0 -2 -4 -6
N = 2630
rho = 0.45
p-value = 5.89E-130
-4 -2 0 2 4
Fold-change (log2) LINE